Geochimica et Cosmochimica Acta 359 (2023) 191–204

Contents lists available at ScienceDirect

Geochimica et Cosmochimica Acta

journal homepage: www.elsevier.com/locate/gca

In-situ phosphate U-Pb ages of the L chondrites

Craig Robert Walton [a,*], Heejin Jeon [b], Ana Černok [c,d,e], Auriol S.P. Rae [f], Ioannis Baziotis [g], Fengzai Tang [h], Venkata S.C. Kuppili [i], Ludovic Ferrière [j], James Darling [k], Sen Hu [l], Martin J. Whitehouse [b], Mahesh Anand [e], Oliver Shorttle [a,f]

[a] University of Cambridge, Institute of Astronomy, Madingley Road, Cambridge, CB3 0HA, United Kingdom
[b] Museum of Natural History, Frescativägen 40, Stockholm, 114 18, Sweden
[c] University of Trieste, Department of Mathematics and Geosciences, Via Weiss 8, 34128 Trieste, Italy
[d] University of Trieste, Department of Mathematics and Geosciences, Via Weiss 8, 34127 Trieste, Italy
[e] Open University, Department of Physical Sciences, Walton Hall, Milton Keynes, MK7 6AA, United Kingdom
[f] University of Cambridge, Department of Earth Sciences, Cambridge, CB2 3EQ, United Kingdom
[g] Department of Natural Resources Management and Agricultural Engineering, Agricultural Univ. of Athens, Iera Odos 75, Athens, 11855, Greece
[h] University of Warwick, WMG, Warwick, CV4 7AL, United Kingdom
[i] Canadian Light Source Inc., 44 Innovation Boulevard, Saskatoon, SK S7N 2V3, Canada
[j] Natural History Museum Vienna, Burgring 7, Vienna, A-1010, Austria
[k] University of Portsmouth, Burnaby Building, Burnaby Road, Portsmouth, PO1 3QL, United Kingdom
[l] Institute of Geology and Geophysics, Chinese Academy of Sciences, Key Laboratory of Earth and Planetary Physics, Beijing, 100029, China

ARTICLE INFO

Associate editor: Tomohiro Usui

Keywords:
Early Solar System
Collision history
Bombardment
L chondrites
Meteorites
U-Pb geochronology

ABSTRACT

The thermal history of asteroids is recorded by the radioisotopic ages of meteorites that derive from them. Radioisotopic ages may date a number of events, such as the cooling of a parent body during waning radiogenic metamorphism, rapid cooling experienced upon parent body break-up, and/or subsequent collision-induced reheating of material. However, sampling statistics for meteorite radioisotope ages are currently relatively low and most are derived from analyses of bulk material, therefore lacking the in-situ microtextural context that aids in distinguishing collisional events. Here, we present new in-situ apatite U-Pb ages for nine L chondrite meteorites using secondary ionisation mass spectrometry.

Our measurements greatly expand the L chondrite phosphate U-Pb age record and provide evidence for distinct stages in the thermal evolution of the L chondrite parent asteroid, including: early collisions driving parent body fragmentation- and/or exhumation-associated cooling at > 4530 Ma; onion-shell-style cooling with waning radiogenic metamorphism until 4500 Ma; late collisional reheating from 4480–4460 Ma; parent body break-up at 474 ± 22 Ma; and recent ejection events within several 10s of Myr of present day. We show that meteorite shock stage correlates with upper intercept age but is uncorrelated with lower intercept age. This outcome links the upper intercept ages alone to the preserved high-energy impact-related features in strongly shocked meteorites, which has important implications for our interpretation of the L chondrite U-Pb record.

We see no evidence in our record for collisional episodes between 3000–4400 Ma, i.e., the Late Heavy Bombardment. Our upper intercept age record hints that collision rates changed as a result of some dynamical instability at 4460–4480 Ma, which may have strongly depleted the main asteroid belt, and/or that L asteroid physical structure changed such that the shock metamorphic response to collisions was muted after this time, e.g., by the formation of weak rubble pile bodies. L chondrite phosphate U-Pb ages provide evidence for a heterogeneous early and shared late (less than 500 Ma) thermal history for the majority of L chondrite meteorites falling to Earth today. From this observation, we infer that most L chondrites derive from a single parent asteroid (in existence from around 4500–4440 Ma to 474 ± 22 Ma), which has since been disturbed to create an asteroid family. Our record of meteorite U-Pb ages traces out the thermal and dynamical evolution of the L chondrite asteroid. These observations can be used in future to benchmark dynamical models of Solar System evolution.

* Corresponding author.
E-mail address: crw59@cam.ac.uk (C.R. Walton).

https://doi.org/10.1016/j.gca.2023.07.012
Received 27 January 2023; Accepted 12 July 2023
Available online 18 July 2023

1. Introduction

A record of the timing and nature of asteroid collisions is delivered to Earth today by meteorites (Dodd and Jarosewich, 1979; Haba et al., 2019; Walton et al., 2022). Meteorites preserve both mineral features that evidence the passage of shock waves and radioisotopic ages that trace thermal evolution over time. This meteorite record of asteroid collisions represents an invaluable empirical constraint on the dynamical evolution of the Solar System, which allows models of planetary orbital evolution to be tested (Nesvorný et al., 2002; Bottke et al., 2015) and the timing of the delivery of a late veneer of volatiles and highly siderophile elements to Earth (Schlichting et al., 2012; Budde et al., 2019). However, meteorites often contain minerals recording complex radioisotopic ages.

Asteroid geochronology is assessed by analysing the radioisotopic compositions of either whole rocks or specific minerals, which accumulate daughter isotopes as long as the phase of interest remains below the closure temperature for daughter-isotope diffusion. Radioisotopic ages in meteorites are therefore largely a record of asteroid thermal evolution. Radiogenic heating will occur through the decay of short-lived radionuclides during an era of parent body thermal metamorphism. As heating from short-lived radionuclides wanes, cooling ages will sequentially be recorded in minerals/rocks according to their respective closure temperatures and sample location within the asteroid. The center regions will remain hotter for longer than the outside, creating an age distribution of radiometrically younger material with depth, i.e., an onion-shell structure (Taylor et al., 1987; Göpel et al., 1994; Trieloff et al., 2003; Gail and Trieloff, 2019; Hellmann et al., 2019).

Collisions may superimpose significant heterogeneity on this simple onion-shell age structure (Davison et al., 2013). Collisions add heat to the asteroid, which allows partial or full reset of previously closed mineral/rock radioisotope systems. Equally, a collision may exhume material that was above its closure temperature to near or at the asteroid's surface, where it may then quickly cool below its mineral/rock closure temperature. Finally, collisions driving textural modification of the asteroid at a meso- and micro-scale, altering the thermal properties of asteroid material and the micro-structure of individual minerals (Darling et al., 2016). As examples of the potential complex age structures that collisions may produce: if a collision occurs when much of a parent body remains hot, material exhumed from depth to a newly shallow location will, upon cooling, record an anomalously young age for its petrologic type; conversely, if a collision occurs after a parent body has already cooled, material reheated above its closure temperature by the collision will record an anomalously young age among all petrologic types.

Some isotopic dating systems employing bulk sample analyses yield complex age distributions consistent with multiple episodes of open system behaviour, e.g., Ar-Ar, Righter et al. (2015). In-situ analyses offer the advantage of correlating age information with specific microtextural or microstructural information, which can help to filter, interpret, or otherwise contextualisecomplex datasets. However, whether in-situ or bulk dating methods are employed, the reconstruction of asteroidal thermal history remains challenging. Different minerals and parent-daughter isotope systems will be more or less well suited to disentangling the heterogeneous age distributions of meteorites.

The apatite uranium-lead (U-Pb) system in particular has great potential as a collisional thermochronometer, due to: (1) the ubiquity of apatite with detectable U and Pb concentrations in many meteorite classes (Jones et al., 2014, 2016), e.g., whilst apatite is generally absent in type 3 ordinary chondrites (Walton et al., 2021), it is present in chondrite petrologic types 4, 5 and 6; (2) typically sufficient grain size to obtain multiple in-situ analyses within an individual apatite grain; (3) generally low common Pb in chondrites; having a moderate closure temperature (apatite: 773 K, Blackburn et al. (2017)), demanding either short-lived high-temperatures or geological timescales of moderate heating (Blackburn et al., 2017) to fully reset; (4) the ability of a suite of grains to record multiple stages of thermal processing, and therefore to untangle complex thermal histories (Mezger and Krogstad, 1997); and, finally, (5) grain-specific occurrence of microtextures (e.g., fractures) which have been shown to correlate with U-Pb isotope ratios, permitting detailed interpretation of upper and lower intercept U-Pb ages on concordia diagrams (Walton et al., 2021, 2022).

Indeed, the use of microtextures to discriminate between competing interpretations of complex U-Pb data reinvigorates asteroid thermochronology as a benchmark of astrophysical models of the dynamical history of the Solar System (Darling et al., 2016; Černok et al., 2021). Crucially, meteorite phosphate U-Pb ages may be able to robustly record collisions at four distinct epochs of Solar System history: ≥ 4530 Ma: Initial asteroid assembly, concurrent with parent body radiogenic metamorphism; 4530–4500 Ma: Asteroid disruption and the start of rubble-pile body formation at around 4530–4500 Ma; 4400–4500 Ma: Possible late dynamical changes (Bottke et al., 2015; Mojzsis et al., 2019); and 4440–0 Ma: Random disrupting collisions (Vokrouhlický et al., 2017; McGraw et al., 2018; Walton et al., 2022).

Despite this great potential, currently available phosphate U-Pb age sampling statistics are insufficient to resolve the details of collision histories witnessed by individual parental asteroids and their derivative families. The L chondrites are the most common undifferentiated meteorites in our museum and lab sample collections, sampling a wide range of collision-induced pressure-temperature histories, superimposed on the background thermal history of the parental L asteroid(s) that is unrelated to shock reheating or disruption-induced cooling (Edwards and Blackburn, 2020). The enrichment of ancient sedimentary rocks (mid-Ordovician limestone, Kunda stage) on Earth in L-type meteorites also indicates their continued disruption over Solar System history (Schmitz et al., 2019). Resolving the U-Pb age distributions of the L chondrites is therefore a priority for unpicking the collision history of the Solar System, which links together important observations, models, and interpretations from astronomy, geology, and meteoritics.

Here, we present in-situ secondary ion mass spectrometry (SIMS) analyses of apatite U-Pb ratios for nine L chondrite samples from museum collections. The specimens from which samples have been prepared were recovered at various points in time – from over 150 to less than 20 years ago. All U-Pb ages are determined by regression analysis of spot analyses of phosphate grains in each meteorite. Efforts were made to obtain multiple spots on individual grains in each case (for exact statistics per sample, please consult File S1). We present microtextural information to contextualise and properly filter U-Pb age data. Samples include weakly shocked through to strongly shocked meteorites (see Methods; Table 1). Our results more than double the number of published phosphate U-Pb SIMS ages for L chondrites, creating the first statistically meaningful population of SIMS U-Pb ages for meteorites derived from a common parent asteroid.

2. Samples and methods

2.1. Sample selection and microscopy

Nine L chondrite samples were selected on the basis of low weathering stage (less than W3; including 4 falls – Château-Renard, Kyushu, Monze, and Peace River) and shock stage (spanning S2 to S6). Polished uncovered thin sections from the Natural History Museums of London, Cambridge (Sedgwick Museum of Earth Science), and Vienna were investigated by optical microscopy for petrographic features considered in published shock stage classification schemes (Stöffler et al., 1991, 2018). Sections were then characterized by Scanning Electron Microscopy (SEM) on a Quanta 650 at the University of Cambridge. Backscattered Electron (BSE) images and elemental maps using Energy Dispersive X-ray Spectrometry (EDS) were collected for each sample in order to identify the distribution of key phases and provide context for higher-magnification analyses. Apatite ($Ca_5(PO_4)_3[OH, Cl, F]$) and merrillite ($Ca_9NaMg(PO_4)_7$) were distinguished on the basis of EDS

measurements in point mode, with 10 s spectral acquisition times, based on the abundance of P, Ca, Na, Mg, and Cl. Panchromatic SEM-Cathodoluminescence (CL) images were collected on selected phosphate and plagioclase grains previously imaged in BSE, in order to obtain an initial view of crystal structure variability (crystallinity, evidence of re-crystallisation, etc.) across the sample.

Lattice orientation, internal microtexture, and structural disorder of selected phosphate minerals were studied by electron back-scatter diffraction (EBSD). EBSD analyses wereundertaken using Oxford Instruments Nordlys-nano EBSD detector mounted on the Zeiss SEM EVO MA10 SEM fitted with a LaB6 electron source at the University of Portsmouth, UK. Data were processed using Oxford Instruments Aztec software, and then further analysis of EBSD data was undertaken using the Channel 5 software suite. Pole figures for merrillite were scaled for whitlockite.

Diffracted electrons were collected at a tilt angle of 70°, using a primary electron beam with 20 kV accelerating voltage and 1 nA probe current in variable-pressure mode (N_2 was used to maintain chamber pressure of 20–30 Pa), following the approach of Darling et al. (2016). Diffraction patterns were automatically captured and indexed every 50–500 nm across manually defined areas. Apatite diffraction patterns were indexed to the chlorapatite crystal lattice parameters of Hughes et al. (1989). Merrillite was indexed against the trigonal crystal parameters of Xie et al. (2015). Wild spike reduction was conducted on all datasets. We iteratively performed zero solution removal up to 4 neighbours to clean datasets. Clear cases of incorrect 180° rotated orientations were manually reversed.

2.2. Apatite U-Pb analysis by SIMS

We exclusively targeted apatite in this study, confirmed beforehand during SEM + EDS sessions. All thin sections were coated with a ~ 30 nm layer of gold. U-Pb dating of apatite was carried out using CAMECA IMS 1280 ion microprobes at the Institute of Geology and Geophysics at the Chinese Academy of Sciences (IGGCAS) in Beijing and the NordSIMS facility at the Swedish Museum of Natural History. Beenham and Château-Renard were analysed at IGGCAS and the other samples at NordSIMS largely following the methods described by Li et al. (2012) and Černok et al. (2021), respectively. Sample Pb/U ratios were calibrated against the NW-1 apatite standard (1160 ± 5 Ma, 2 σ) using a power law relationship between measured $\frac{^{206}Pb^*}{U}$ (where * denotes the radiogenic fraction) and $\frac{UO}{U}$ (IGGCAS) or $\frac{Pb}{U}$ and UO_2/U ratios (NordSIMS).

The duoplasmatron-generated O_2^- primary ion beam was accelerated at ~ 13.8 kV and illuminated through an aperture to create a 10 × 15 μm spot with a current of 10–12 nA at IGGCAS and 13 kV with a current of 1.7–5.3 nA at NordSIMS. The Hyperion H201 RF Plasma source was used to generate a critically focused O_2^- primary beam with 13 kV, which was tuned to 1.7–5.3 nA and rastered over an area of 5 × 5 μmm during analysis at NordSIMS.

Multi-collector mode was used at IGGCAS, with $^{204}Pb^+$, $^{206}Pb^+$, and $^{207}Pb^+$ were simultaneously collected detected with electron multipliers L2, L1 and C, respectively. Then $^{238}U^+$, and $^{232}Th^{16}O^+$, $^{238}U^{16}O^+$ and $^{238}U^{16}O_2^+$ (Li et al., 2012) detected with L1, H1, and H2, respectively on peak hopping. Mono-collector mode was used at NordSIMS: all species were measured on a single multiplier. The $^{40}Ca_2^{31}P^{16}O_3^+$ peak was used as a reference peak for centering the secondary ion beam as well as for making energy and mass adjustments on both instruments. Data reduction was performed using in-house developed software at NordSIMS and the Excel add-in Isoplot. Final reported U-Pb concordia intercept ages were calculated using IsoplotR (Li et al., 2012; Vermeesch, 2018). Further details can be found in (Zhou et al., 2013).

In making analyses, we targeted grains that lacked visual evidence of containing inclusions of other phases – aiming to eliminate contamination of Pb from non-phosphate phases. As an extra check, for each analysis we monitored CaPO count rates, to ensure that the integrated U and Pb counts were coming from phosphates and not other included phases. For all analyses, we pre-sputtered grains with the ion beam for 80 s to remove the Au coat and minimise surface contamination prior to data collection. Where detected with the ^{204}Pb beam, a common Pb correction was applied assuming a present day Stacey-Kramers composition (Stacey and Kramers, 1975; Unruh, 1982). High common-Pb spot compositions that correct poorly (around > 15% common Pb on the basis of ^{204}Pb), were excluded from regression analysis.

We also intentionally targeted both pristine and fracture-damaged regions of phosphate grains, aiming to place multiple spots on any given studied grain. This decision was made on the basis that fracture-damaged grains show the most discordant U-Pb isotopic compositions in previous in-situ U-Pb studies of chondritic phosphates (Walton et al., 2022). In order to ensure that results from NordSIMS and IGGCAS are comparable and reproducible when using our analytical approach, we repeated our previously published analysis of our sample of the Chelyabinsk light lithology (Walton et al., 2022) with the IGGCAS instrument at NordSIMS, targeting both pristine and fractured phosphate domains – some that had been previously analysed and others that were completely fresh.

2.3. Compilation of meteorite shock age and shock stage data

Textural evidence of ancient collisions is often classified using the shock stage scheme (Stöffler et al., 1991; Fritz et al., 2017; Stöffler et al., 2018; Baziotis et al., 2023), and provides some context for age data obtained from a given sample. We applied a set of classification rules to our samples and literature data that are of specific relevance to the phosphate U-Pb system.

Petrologic type 7 and impact-melt samples are assigned shock stage 6 (highest possible; note that this supersedes annealing effects that may result in low shock stage if judged solely on the basis of e.g., silicate mineral features); more recent classifications take precedence, owing to the advancement over time in both the classification scheme itself (Stöffler et al., 1991, 2018) and the methods available with which to assess shock-related mineral features. Samples with spatially variable shock stage (e.g., S4–6 samples, such as Chelyabinsk) are given a single shock stage classification of 5, on the basis that observations to date suggest a comparable outcome for the apatite U-Pb system in S4–6 breccias as in meteorite samples that are uniformly S5 (Walton et al., 2022). This is likely due to the fact that, whilst not texturally equilibrated, the different lithologies of melt-bearing S4–6 breccias thermally equilibrated during the long tail of post impact cooling, sufficient to reset U-Pb ages throughout the rock (Walton et al., 2022).

Applying the above rules, we then group meteorites into strongly shocked (greater than S4) and weakly shocked (S4 and lower). This split approximates the conditions above and below the threshold for significant phosphate Pb age resetting, as determined on the basis of Pb diffusion modelling (Blackburn et al., 2017). Our approach simplifies the presentation of the shocked meteorite record and provides a logical and coherent basis on which to define, compare, and interpret sub-groups of phosphate U-Pb ages. Details of shock stage information for each sample either newly studied here or considered in our metadata analysis are summarised in Table 1. We use a condensed format that conveys the details given in Stöffler et al. (2018). A succinct summary of the classification criteria is presented below.

Effects resulting from local pressure-temperature excursions, with onset at S3, are grouped into categories M1–3: [M1] opaque shock veins; incipient formation of melt pockets (S3); [M2] melt pockets, interconnected melt veins; opaque shock veins (S4); [M3] pervasive formation of melt pockets, veins, and dikes, opaque shock veins (S5 and above).

Shock features recorded by olivine, with onset at S1 and incrementing in line with overall shock stage, are grouped into categories O1–7: [O1] sharp optical extinction; [O2] undulatory extinction; [O3] planar fractures; [O4] weak mosaicism; [O5] strong mosaicism; [O6] local

Table 1
Shock-feature classification of L chondrites: Features reported in the literature are referenced. The symbol '*' denotes observations made in the course of this work. The symbol 'X' denotes a classification by inference made in this work on the basis of literature reports. The symbol '–' denotes any feature not reported. LIM: L-type impact melt. All shock stages are reported according to the convention of Stöffler et al. (2018). Shock classification types M and O – derivative of Stöffler et al. (2018) – are detailed in the Methods. Rwd: ringwoodite. Wds: wadsleyite. Jd: jadeite. Brg: bridgemanite.

Sample	Shock stage (S1–7)	Melt features (M1–3)	Olivine features (O1–7)	High Pressure Phases (HPPs)
This work				
Château-Renard (L6)	S5 (Baziotis et al., 2018)	M3 (Baziotis et al., 2018)	O5 (Baziotis et al., 2018)	Rwd, Wds (Baziotis et al., 2018)
McKinney (L4)	S5 *	M3 *	O3 (Baziotis et al., 2018)	–
Alfianello (L6)	S5 (Gattacceca et al., 2014)	M2 *	O4–5 *	–
Peace River (L6)	S5 *	M3 *	–	–
Kyushu (L6)	S5 (Bischoff et al., 2018)	M2 *	–	–
Monze (L6)	S4 (Xie et al., 2001)	M2–3 (Bischoff et al., 2018)	–	–
Lincoln County (L6)	S4 (Bischoff et al., 2018)	M1 (Bischoff et al., 2018)	–	–
Beenham (L5)	S3 (Bischoff et al., 2018)	M1 *	–	–
Indianola (L5)	S3 *	M1 *	–	–
Literature				
NWA 11042 (LIM)	S6 | S5 (Wu and Hsu, 2019)	M3 (Wu and Hsu, 2019)	O5 (Wu and Hsu, 2019)	Rwd (Wu and Hsu, 2019)
Novato (L6)	S4–6 (Yin et al., 2014)	M3 (Yin et al., 2014)	–	–
Sahara 98222 (L6)	S4–6 (Bischoff et al., 2018)	M2 (Yin et al., 2014)	–	Wds, Jd (Yin et al., 2014)
NWA 7521 (LIM)	S6 | S4–6 (Li and Hsu, 2018c)	M3 (Li and Hsu, 2018c)	O4	–
Suizhou (L4)	S4–5 (Xie et al., 2001)	M2 (Li and Hsu, 2018a)	O4 (Li and Hsu, 2018a)	Rwd, Brg (Li and Hsu, 2018a)
Sixiangkou (L5)	S5 X	M3 (Li and Hsu, 2018b)	–	Rwd, Jd (Li and Hsu, 2018b)
Knyahinya (L5)	S4 (Gyollai et al., 2009)	–	O4 (Gyollai et al., 2009)	–
Ausson (L5)	S3 (Gattacceca et al., 2014)	–	–	–
Homestead (L5)	S4 (Gattacceca et al., 2014)	–	–	–
Barwell (L6)	S3 (Gattacceca et al., 2014)	–	–	–
Ladder Creek (L6)	S2–3 (Blackburn et al., 2017)	M1 (Blackburn et al., 2017)	O2–3 (Blackburn et al., 2017)	–
Bruderheim (L6)	S4 (Blackburn et al., 2017)	M1 (Blackburn et al., 2017)	O4 (Blackburn et al., 2017)	–
ALH 85026 (L6)	S4 (Blackburn et al., 2017)	–	O2–3 (Blackburn et al., 2017)	–
Marion (L6)	S2–3 (Blackburn et al., 2017)	–	–	–

melting and recrystallisation of olivine; [O7] whole-rock melting. The presence/absence of high-pressure-phases (HPPs) is also noted.

For samples with complex shock histories that can be placed into a robust sequence, the chronology of shock stages achieved by the sample are indicated as follows: S6 | S5, i.e., first S6 (whole-rock shock-melting) then, at some later time, shocked again to S5 (partial shock-melting).

2.4. Statistical comparison of U-Pb age distributions

A key part of this study is evaluating whether U-Pb ages from different groups of meteorite samples have the same age distribution. To perform this test, we calculated the maximum difference between the empirical cumulative distribution functions for different populations of ages, and applied the 2-sided Kolmogorov–Smirnov (KS) test to calculate a p-value from this. The null hypothesis being tested is that the observed data populations are drawn from the same underlying distribution.

Some level of difference would be expected between samples from two identical populations not only due to finite sample sizes, an effect the K-S statistic is designed to capture, but also due to the measurement error on the data, an effect the standard K-S statistic does not capture. We account for this fuzziness in the statistic by re-sampling the individual data points according to their uncertainty to create new samples of the populations, these are then randomly shuffled, and split to create two new sample groups for re-application of the KS test. This was performed 10,000 times. By assessing the proportion of these randomised populations that gave KS statistics higher than the original KS value, we determined the probability of the null hypothesis being true, i.e., that the observed populations, now accounting for measurement error, are the same as one another.

For statistical comparison, samples were initially split into strongly (>= S5) and weakly (<= S4) shocked groups, on the basis that this demarcates the boundary for significant perturbation of phosphate U-Pb upper intercept ages (see above for further details). We further divide samples on the basis of their petrologic types. L6 samples are the most heavily sampled type of L chondrite for phosphate U-Pb and Pb-Pb ages ((Blackburn et al., 2017), Table 1). Given that samples of similar petrologic type must have experienced similar histories of parent body thermal metamorphism – not withstanding subsequent shock processing – we define two L6 groups, one of weakly and one of strongly shocked meteorites. Owing to small sampling statistics ($n = 4$) for strongly shocked samples of lower petrologic type, we group non-L6 meteorites together (i.e., L4, L5, and L7) and divide between weakly and strongly shocked. By comparing these L chondrites sample groups, we can gain insight into the degree to which shock history results in statistically significant differences in radiometric reset (i.e., thermal) history recorded by otherwise similar groups of L chondrites. Details of all samples studied including sample IDs and observed shock features are provided in Table 1.

3. Results

3.1. U-Pb isotope analyses

Extended details of U-Pb isotopic data generated in this study are presented in the Supplementary Material (Table S1) – including a comparison of the analysis of Chelyabinsk (LL5) at NordSIMS to previously published results in Walton et al. (2022), which shows that the two data-sets yield identical upper and identical lower intercept ages, within error. This outcome supports inter-lab comparability of our results. Our samples are largely clean with respect to common Pb ($f_{206} < 1\%$). In many cases ^{204}Pb, a non-radiogenic Pb isotope, was not detected (analyses recording ^{204}Pb intensities at $< 3\times$ the average detector background, compared to signals on ^{206}Pb many times the detector background). Where common Pb was detected, correction assuming a terrestrial composition was successful, i.e., producing compositions within 2 σ error of concordant or lying along the same single linear regression line as spot compositions where common Pb was not detected (see Supplementary Material Table S1). Common-Pb-rich compositions plot close to the terrestrial common Pb composition of Stacey and Kramers (1975) (Supplementary Figs. S1–S6).

Fig. 1 shows all in-situ U-Pb data generated in our study plotted on Wetherill concordia diagrams. All of our L chondrite samples return some concordant compositions except for Château Renard (L6,

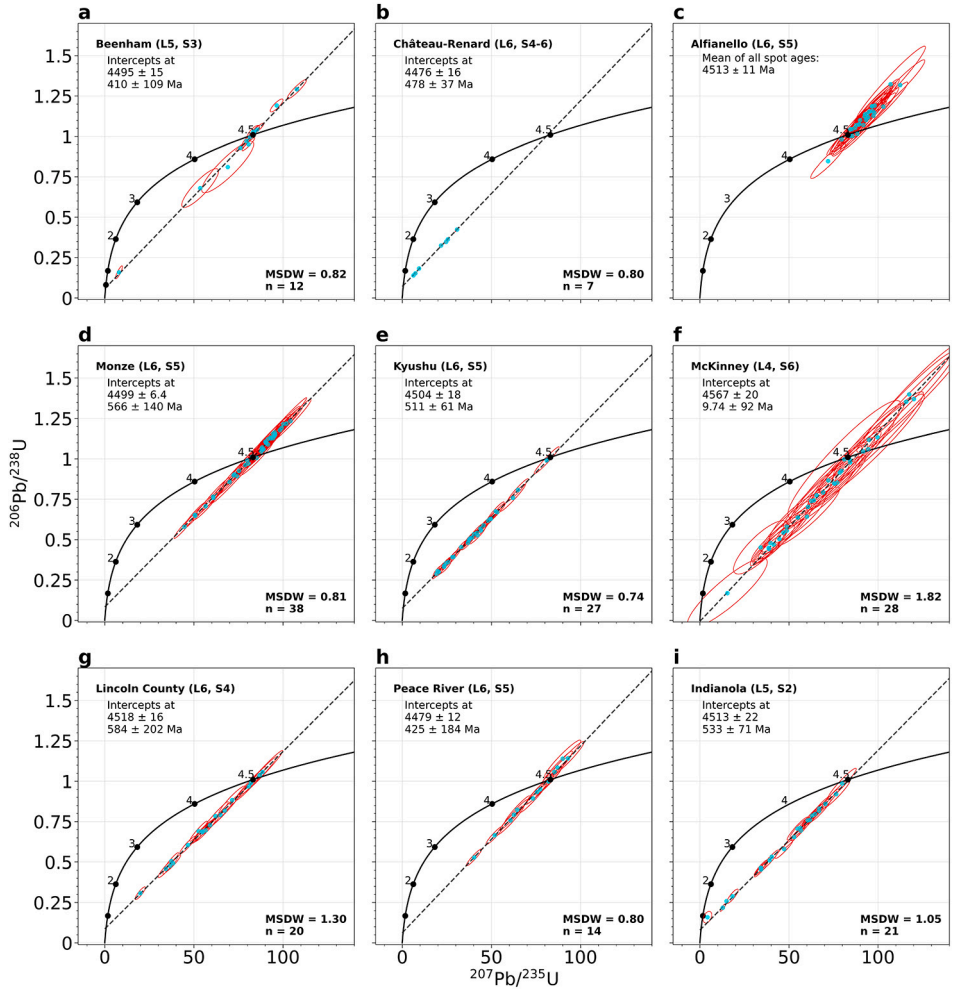

Fig. 1. Concordia plots of apatite U-Pb compositions in L chondrite meteorites. Each data point is shown with 2 σ error ellipse.

S4–6; Fig. 1b) in which we only found discordant grains. This spread of Pb/U ratios enables us to calculate upper and lower concordia intercept U-Pb ages for all of the meteorites analysed. Data from any given sample fall along a single linear array, yielding well-constrained upper intercept ages (2 σ uncertainty of around 10–20 Myr) and moderately- to poorly-constrained lower intercept ages (2 σ uncertainty of around 10–100 Myr).

The exception to this pattern is Alfianello (L6, S5), for which data are mostly within error of concordant and yet are systematically offset in the direction of Pb-gain, i.e., displaying slight reverse discordance. Only one data point is resolvably discordant, i.e., not within 2 σ error of the concordia and located in discordant phase space. In this instance, we report the youngest concordant $\frac{^{207}Pb}{^{206}Pb}$ age instead of $\frac{^{206}Pb}{^{238}U}$, following Li and Hsu (2018a).

Other samples also display slight reverse discordance, but only along the same linear array as spot compositions that show normal discordance, i.e., the U-Pb compositions of phosphates we have studied, where they show sufficient scatter to be regressed, do not significantly deviate from lying along a single linear array (MSWD ranges from 0.45–1.3). Reverse discordance may represent some unknown process of Pb-gain or U-loss, perhaps related to the same event(s) that cause Pb-loss and normal discordance. This would be consistent with our previous study of Chelyabinsk (LL5), where apatite grains with visible fracture-damaged domains were found to be either discordant or reversely discordant (Walton et al., 2022). Our new results therefore suggest a role for local grain environment in the origin of discordance in ordinary chondritic apatite grains in general.

3.2. Regression of U-Pb data: upper intercept ages

We calculate both concordia intercept U-Pb ages, using all data (after filtering), as well as weighted mean Pb-Pb ages using only data that are concordant within error. In all cases, we find that concordia intercept U-Pb and weighted mean Pb-Pb ages are within error of one another (see Supplementary Material Table S1). This result suggests that ages measured with in-situ SIMS and bulk phosphate isotope-dilution-thermal-ionisation-mass-spectrometry (ID-TIMS) may be comparable. Fig. 2 presents the upper intercept ages calculated in the present study in context of previously published SIMS and ID-TIMS ages. These ages are plotted separately; no results obtained with different techniques have been combined or averaged.

In order to interpret phosphate U-Pb ages, it is crucial to determine whether or not there are any apparent relationships between indicators of meteorite shock metamorphism (shock stage) and preserved phosphate U-Pb ages. We group our samples into weakly ($\leq$ S4) and strongly ($\geq$ S5) shocked (Fig. 4). This division captures the distinction between samples that preserve petrological evidence of shock heating consistent with the conditions needed to reset the phosphate U-Pb system, i.e., shock stage 5 and above (see methods and previous subsection). We find that weakly shocked meteorites preserve upper intercept U-Pb ages consistent with the end of parent body radiogenic metamorphism, i.e., for the L chondrite parent body, around 4550–4500 Ma (Blackburn et al., 2017; Edwards and Blackburn, 2020). Importantly, this result demonstrates that the phosphate U-Pb system as measured by SIMS returns U-Pb ages consistent with Pb-Pb ages calculated from ID-TIMS analyses

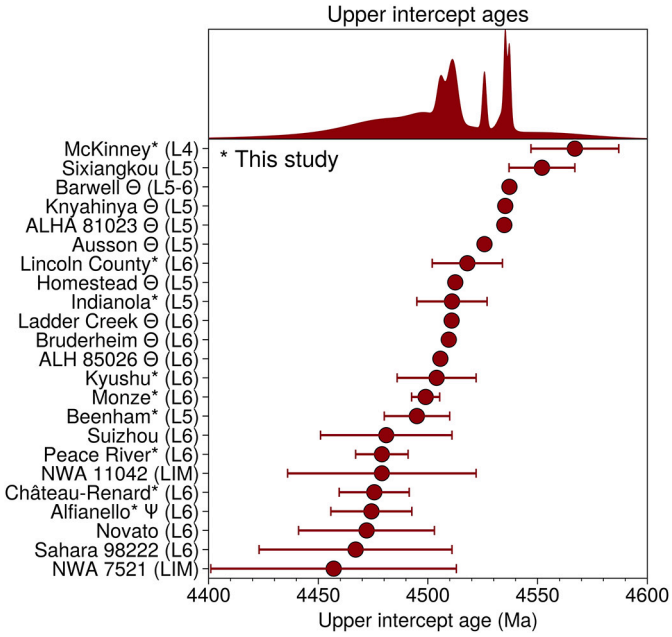

Fig. 2. Upper intercept phosphate U-Pb and Pb-Pb ages of L chondrite meteorites: Samples are in descending order of calculated upper intercept U-Pb age. Error bars are all 2 σ. Also included are $\frac{^{207}Pb}{^{206}Pb}$ ages; those measured by ID-TIMS are denoted by the symbol Θ and SIMS results denoted by the symbol Ψ – Alfianello only. All other ages are $\frac{^{206}Pb}{^{238}U}$ ages. Literature results are included from Yin et al. (2014); Li and Hsu (2018a,c,b); Wu and Hsu (2019); Blackburn et al. (2017); Göpel et al. (1994); Ozawa et al. (2007).

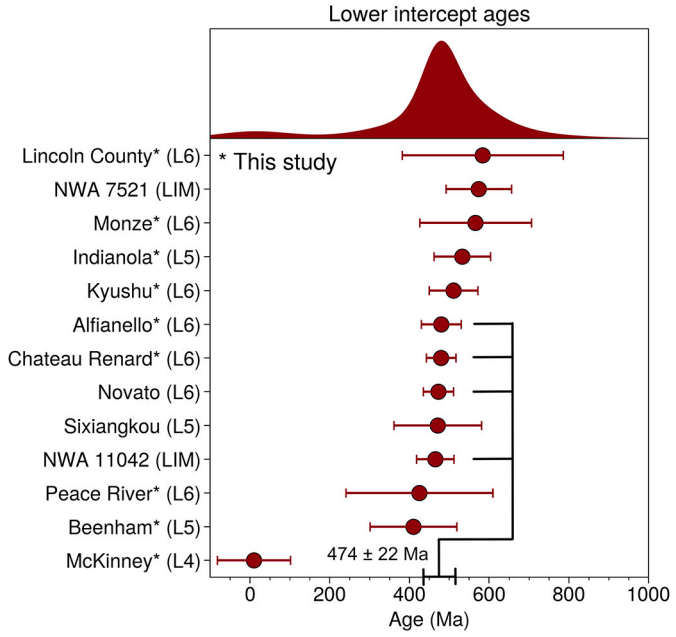

Fig. 3. Lower intercept ages of L chondrite meteorites: Samples are in descending order of calculated lower intercept U-Pb age. A stacked gaussian probability distribution is shown in the top panel. Error bars are all 2 σ. Also included are literature results from Li and Hsu (2018b,c); Wu and Hsu (2019); Yin et al. (2014). The mean age of all lower intercepts with uncertaintites of 50 Myr or less is shown.

of whole phosphate grains from petrologically comparable meteorite samples.

Strongly shocked meteorites return phosphate U-Pb upper intercept ages that range from older to younger than weakly shocked meteorite ages. Shocked meteorite U-Pb ages sparsely sample the period of time from 4600–4500 Ma but sample the period of time 4500–4450 Ma with comparatively high frequency. One sample, McKinney (L4) returns an upper intercept age (4567 ± 20 Ma) that is among the oldest phosphate U-Pb or Pb-Pb ages ever reported (Göpel et al., 1994; Terada and Bischoff, 2009; Yin et al., 2014; Blackburn et al., 2017; Li and Hsu, 2018a,c; Edwards and Blackburn, 2020; Walton et al., 2022).

Statistical tests demonstrate with a high degree of confidence ($p = 0.05$) that highly and weakly shocked L chondrite U-Pb upper intercept populations are not drawn from the same underlying distribution (Fig. S7). This outcome holds true when comparing sub-populations of weakly and strongly shocked meteorites, e.g., weakly vs. strongly shocked L6 chondrites, or weakly vs. strongly shocked non-type-6 L chondrites (Fig. S7).

3.3. Regression of U-Pb data: lower intercept ages

Fig. 3 presents lower intercept U-Pb ages for all samples for which observed discordance permits the calculation of a statistically valid linear regression (Vermeesch, 2018). In cases where there is only weak discordance, the error on the lower intercept is large. This follows from the expected behaviour that including strongly discordant grains in a regression – if laying on the same linear array – will greatly increase lower intercept age error precision and accuracy, e.g., as demonstrated by our previous analyses of the Chelyabinsk meteorite (Walton et al., 2022). We can be confident that the lower intercept ages recovered in this study are meaningful for two reasons. First, our lower intercept ages are calculated using broadly normally discordant data that is unlikely to result from contamination (Unruh, 1982). Second, these lower intercept ages are within error of ancient sediments on Earth that are known to be strongly enriched in fossil L meteorites, providing an independent line of evidence for a collisional event involving the/a L chondrite parent body at this time (Schmitz et al., 2019).

All lower intercept ages that have 2 sigma error greater than 100 Myr are both within error of one another and the more tightly constrained lower intercept ages, e.g., Peace River vs. Novato (Yin et al., 2014). The precision of these ages might be improved with dedicated sampling campaigns hunting for extremely discordant grains, but due to our analytical approach and resulting well-constrained discordia, any such result would be to refine our calculated ages by the order of tens rather than hundreds of Myr.

We find that lower intercept ages display no relationship with shock stage (Fig. 5). Performing an identical statistical comparison to that conducted with sub-populations of L chondrite upper intercept ages, we find that there is no difference in the distribution of lower intercept ages for weakly versus strongly shocked samples (Fig. S8). This outcome links upper intercept ages alone to preserved shock features, which has several important implications for our interpretation of the L chondrite U-Pb record.

3.4. Quantifying phosphate response to shock metamorphism

In previous sections we grouped results for different meteorites based on shock stage (reported or assessed in this study). This grouping is reasonable to aid in interpreting U-Pb ages only if we assume that shock stage provides reliable information about the peak pressure and temperature conditions experienced by phosphates in a given meteorite sample. Resetting of the phosphate U-Pb system is driven by diffusion – a temperature-dependent process that can be enhanced by the development/presence of shock-induced microstructures (Černok et al., 2021). Threshold shock stages for phosphate U-Pb system resetting on the basis of heat-driven diffusion alone and a pristine crystal lattice have been calculated by Blackburn et al. (2017), providing the basic condition by which we split meteorite samples for statistical comparison in later sections of this manuscript. However, given that Pb-diffusion out of phosphate crystal lattices may be promoted by shock-induced microstructures, it is important to check that the basis on which we have

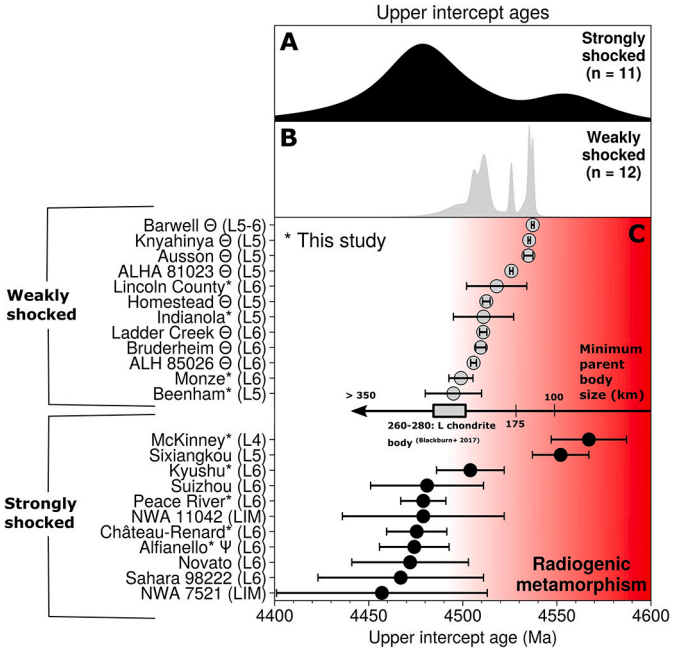

Fig. 4. Upper intercept phosphate U-Pb and Pb-Pb ages of L chondrite meteorites: Error bars are all 2 σ. Also included are $\frac{^{207}Pb}{^{206}Pb}$ ages, with those measured by ID-TIMS (Blackburn et al., 2017) denoted by the symbol Θ and SIMS results denoted by the symbol Ψ – Alfianello only. All other ages are $\frac{^{206}Pb}{^{238}U}$ ages. Literature results are included from Yin et al. (2014); Li and Hsu (2018a,c,b); Wu and Hsu (2019); Blackburn et al. (2017); Göpel et al. (1994); Ozawa et al. (2007). Samples are grouped into weakly and strongly shocked, i.e., whether or not, according to preserved shock features, collisional heating was sufficient to have measurably perturbed the phosphate U-Pb system. Stacked gaussian probability density functions for each population are shown in panels A and B. LIM: L-type impact melt-rock. L5–6: transitional between petrologic types 5 and 6. Indicated along the central arrow is the estimated minimum parent body size needed to obtain a progressively younger central L6 Pb-phosphate date (Blackburn et al., 2017; Edwards and Blackburn, 2020). Samples analysed in this study are indicated with the symbol '*'. Knyahinya is a transitional sample, with a classification of L/LL5.

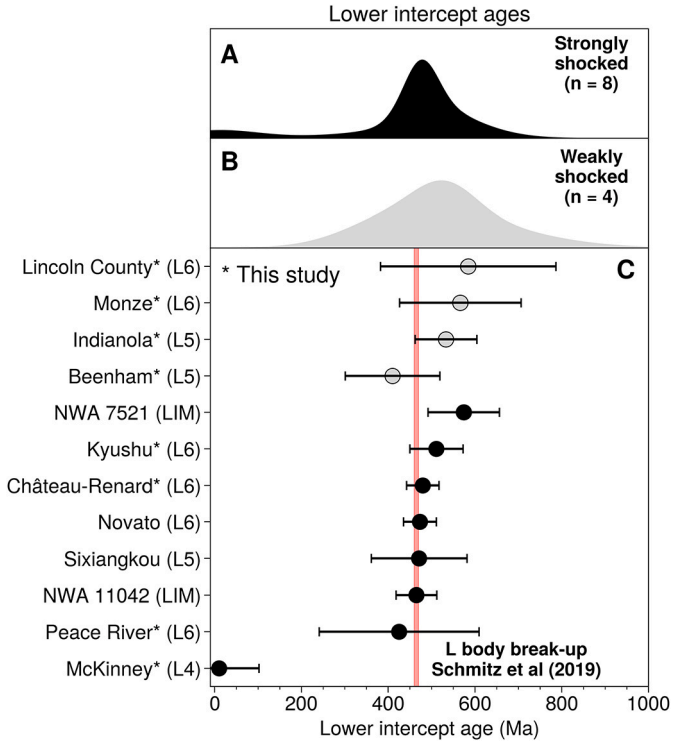

Fig. 5. Lower intercept ages of L chondrite meteorites: Most samples are within error of one another and within error of 466 ± 1 Ma – the age of a previously discovered Ordovician sedimentary deposit rich in fossilised L chondrite meteorites (Schmitz et al., 2019). Samples are grouped into weakly (≤ S4) and strongly (≥ S5) shocked, i.e., whether or not, according to preserved shock features, collisional heating was sufficient to have measurably perturbed the phosphate U-Pb system. Stacked gaussian probability distributions for each population are shown in panels A and B, calculated using the probability density function assuming a normal continuous random variable with the scipy package. There are fewer ages reported here than in Fig. 1 owing to the fact that now all L chondrite meteorite phosphate suites appear to record discordant U-Pb isotopic compositions, precluding the calculation of a statistically valid lower intercept age. The age of the L body break-up event inferred on the basis of fossil-L-meteorite-rich sedimentary beds by Heck et al. (2017) and Schmitz et al. (2019) is indicated with a solid red annotated line. Also included are literature results from Li and Hsu (2018b,c); Wu and Hsu (2019); Yin et al. (2014).

split samples is self-consistent with other criteria for doing so – in particular, the presence/absence and degree of development of shock-induced microstructure in apatite has been largely unstudied in chondrites and therefore not yet properly included within existing shock stage schemes.

CL images return little information about the extent of crystal plastic deformation experienced by a phosphate grain, but readily record evidence for recrystallisation (Walton et al., 2021). Prior to SIMS, we checked at least several apatite grains eventually analysed from each sample in our study with CL. None of the apatite grains analysed in this study returned visible evidence for recrystallisation (but many merrillite grains did in samples ≥ S4, e.g., Isoulane-n-Amahar; Fig. 7). For phosphate grains that we were able to index, EBSD unambiguously reveals the presence/absence and degree of crystal plastic deformation. We analysed apatite grains in the dark (S5) lithology of Chelyabinsk (LL5) and McKinney (L4, S6). Added to our previous analyses of the Chelyabinsk light lithology (S4; Walton et al. (2021)), these samples span shock stages S4, S5, and S6, i.e., the critical window for U-Pb resetting when solely considering heat-driven Pb-diffusion (Blackburn et al., 2017).

We find that crystal plastic deformation is evident for apatite grains in shocked L chondrites (as classified using the scheme of Stöffler et al. (2018)), but to varying extents. S4 apatites in Chelyabinsk have crystal plastic deformation misorientations of 10° (Walton et al., 2021). S5 apatites have misorientations of up to 30° (Fig. S10). S6 apatites have misorientations of up to 40° (Fig. 6). These results are consistent with analyses of lunar shocked apatite grains reported by Černok et al. (2019) and terrestrial apatites shocked during hypervelocity impacts as reported by Kenny et al. (2019). This consistency in apatite's response to shock-wave passage through chondrites and lunar rocks of similar shock stage suggests that bulk shock stage is a reasonably widely applicable metric of PT conditions. For our purposes, it also supports the use of shock stage to interpret phosphate U-Pb ages in terms of collisional metamorphism.

4. Discussion

4.1. Radiogenic versus impact-induced heating of L chondrites

Our results reveal statistically significant differences between the upper intercept ages of strongly versus weakly shocked L chondrites (Fig. S7). Meanwhile, we find no such difference between the lower intercept ages of strongly versus weakly shocked L chondrites (Fig. S8). This critical observation is consistent with diffusion models in which complete resetting of phosphate upper intercept U-Pb ages requires metamorphism to shock stage S5 or above (Blackburn et al., 2017), as well as previous suggestions that lower intercept ages may be reset during relatively mild shock events (Walton et al., 2022). Overall, most high-energy shock features in L chondrites are instead dated robustly by upper intercept ages. Lower intercept ages, whilst meaningful,

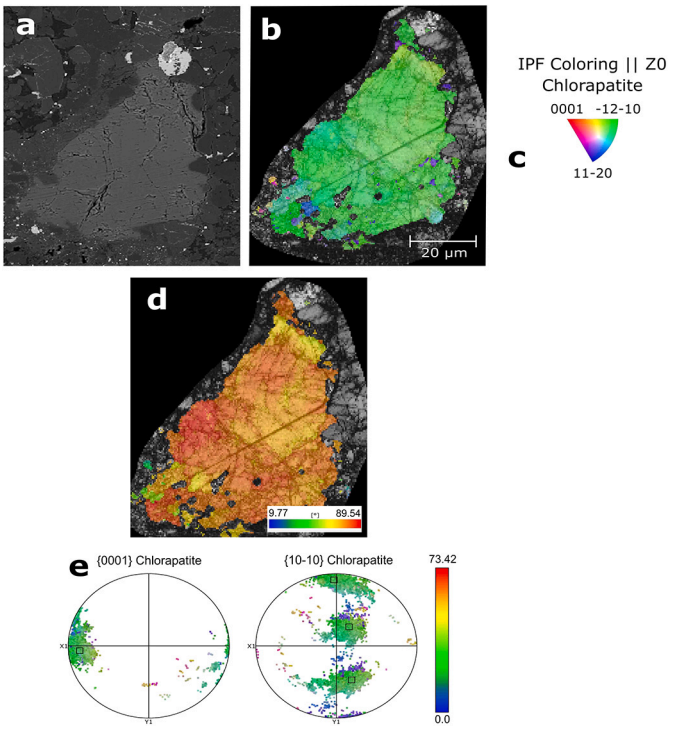

Fig. 6. BSE + EBSD results for apatite in McKinney (L4, S6). a) BSE image of apatite grain in McKinney, adjacent to quenched shock-melt. b) Inverse Pole Figure (IPF) map, revealing one single grain. c) IPF orientation colour key. d) Texture Component map revealing significant crystal plastic strain across the grain. e) Pole figure colour-coded by IPF orientation with respect to an arbitrary reference point on the target grain.

are broadly related to relatively low-energy features, e.g., overprinting fractures (Walton et al., 2022). By relating solely upper intercept ages to shock stage, we are able to untangle the nature of L chondrite parent body radiogenic versus shock-induced thermal evolution.

One key implication of our results is that the majority of strong shock related features in L chondrites date back to early Solar System history (Yin et al., 2014). Meanwhile, our results support previous findings that phosphate upper intercept U-Pb ages from weakly shocked meteorites are a robust archive of the thermal evolution of asteroid parent bodies, recording their onion-shell cooling with the waning of endogenous radiogenic heat sources (Göpel et al., 1994; Blackburn et al., 2017; Edwards and Blackburn, 2020). The youngest upper intercept ages we obtain from weakly shocked meteorites are consistent with an estimated minimum size of the L chondrite parent body (Blackburn et al., 2017) of 260–280 km in diameter. This estimate is derived from models that couple chondritic apatite Pb-diffusion to a parent-body-size-dependent radiogenic heating history (Blackburn et al., 2017). This argument is bolstered by broad consistency between the ages determined from U-Pb SIMS and Pb-Pb ID-TIMS (Fig. 4). Future work should seek to obtain paired ID-TIMS and SIMS analyses of the same samples, in order to fully validate this comparison.

There are caveats to the interpretation of upper intercept ages in strongly shocked meteorites as recording the formation of shock-features in L chondrites. One nuance to consider is how readily material will have been excavated from the parent body into the rubble pile object, which is presumably what is responsible for supplying L chondrites to Earth today. Deeply buried material, which will be a higher petrologic type, requires significant collisional energy to exhume: either a few large events, or many small events. If deeply buried material cooled through the phosphate Pb-closure temperature late – say, 4480 Ma, as is permitted by the higher estimates of chondrite parent body size (Fig. 4; Blackburn et al. (2017)) – then the correlation of textural evidence of strong shock with young phosphate upper intercept U-Pb ages might

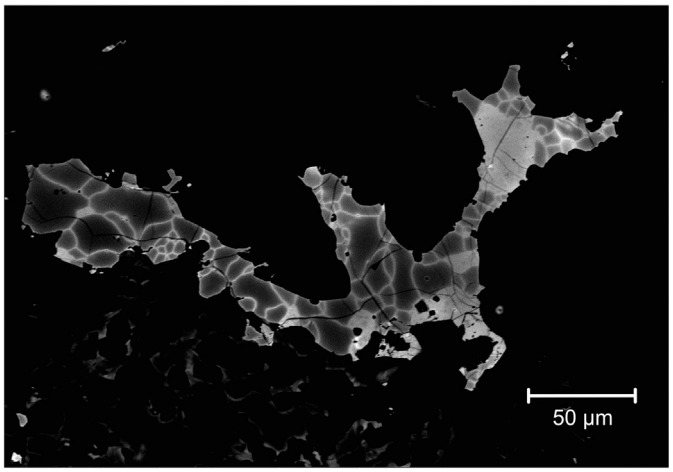

Fig. 7. Recrystallised phosphate (merrillite) in Isoulane-n-Amahar (L6).

emerge in the data without the shock event itself being what is dated. That is, phosphate U-Pb system age and meteorite shock stage would in this scenario be independent of each other but linked by a parent-body-depth dependence.

Nine of the twelve reported upper intercept ages for strongly shocked L meteorites (Fig. 4) are younger than 4490 Ma. Ages this young, if related solely to onion shell thermal evolution, require derivation from the center of an asteroid around 350–400 km in diameter (Fig. 4). This may or may not be inconsistent with parent body size constraints from the ages of weakly shocked L6 chondrites (see above), given that the L6 zone may encompass a large range of depths (Blackburn et al., 2017). Therefore, either strongly shocked L chondrites derive solely from deep late-cooled portions of now-disrupted L-type bodies (Edwards and Blackburn, 2020), in which case the timing of formation of their shock ages remains obscure, or that strongly shocked meteorites indeed record collisional reheating of the materials that they sample.

Our statistical tests can speak to these two hypotheses for the shock stage-age relationship. Comparing the distribution of ages between strongly shocked non-L6 and L6 samples showed them to have indistinguishable age spectra (Fig. S7a). In contrast, weakly shocked L6s have distinct upper intercept ages from each other. This outcome suggests strongly shocked meteorite ages record collisions rather than onion-shell cooling ages. Future work should further interrogate this point by increasing data availability for non-L6 meteorites.

A further caveat to our findings is the possibility that shock-induced microstructures may plausibly lower the shock stage boundary for Pb-diffusion from the apatite crystal lattice. This could move the boundary for resetting from S5, as considered in our statistical comparison of strongly versus weakly shocked meteorites, to S4 or below. Evidently partial reset can occur at much lower shock stage: we have measured lower intercept ages produced via phosphate Pb-loss in an S2 sample (i.e., Indianola). As such, it is clearly possible for relatively weak episodes of collisional metamorphism to at least partially reset chondritic phosphate U-Pb ages, as has been observed in some lunar samples (Černok et al., 2021). Shock-induced microstructures formed at earlier times may provide a coherent explanation for the relative ease with which late Pb-loss can occur at mild conditions (Reddy et al., 2014; Erickson et al., 2015; Blackburn et al., 2017; Černok et al., 2021; Walton et al., 2022). However, the variation in extent of Pb-loss and the exact mechanisms involved are not fully understood.

One plausible mechanism of Pb-loss is via grain boundaries developed during grain recrystallisation. Recrystallisation dissipates strain accumulated during shock wave passage. Analysis of Pb-rich domains located within sub-grain boundaries in recrystallised phosphates may then return elevated Pb concentrations. However, our EBSD and CL

analyses do not provide any evidence for recrystallised apatite generations (i.e., relict parent grains comprised of strain-free subgrains) in our samples. We have observed phosphate recrystallisation in other shocked ordinary chondrites, e.g., Isoulane-n-Amahar – Fig. 7; Chelyabinsk – Fig. S9, Walton et al. (2022)) using the same methods, and so we tentatively rule out this mechanism. Lead-loss could also occur during partitioning into micro-scale apatite-normative melts which, upon crystallisation, will preserve elevated Pb-concentrations. However, as above, our EBSD and CL analyses do evidence any apatite grains having grown from shock melts, i.e., igneous-textured and/or strain-free.

Instead, a mechanism that we proposed in a previous study of the Chelyabinsk (LL5, S4–6) chondrite to explain late apatite Pb-loss may be responsible: grain-damage during fracturing. This phenomenon occurs from low shock stages and correlates with normal discordance in Chelyabinsk apatite grains (Walton et al., 2022). We intentionally targeted some damaged grain regions in the present study. Given the evidence from Chelyabinsk, the same simple and plausibly universal mechanism may be relevant for explaining late Pb-loss from apatite grains in L chondrites, even at low shock stages.

4.2. Solar System dynamics from 4.56–4.40 Ga

Weakly shocked meteorites have a tighter range of phosphate upper intercept U-Pb ages than strongly shocked L meteorites: 45 Myr (from 4495–4540 Ma) versus 100 Myr (from 4460–4560 Ma). Our results suggest that collisional reworking may have caused parts of the L parent asteroid to be exhumed and to cool quickly, producing e.g., the early phosphate U-Pb age of the strongly shocked McKinney and Sixiangkou meteorites (Fig. 4 and 8). However, the error on the age of McKinney is relatively large, and overlaps with the upper age range of that expected to be recorded by L4 samples in general (Gail and Trieloff, 2019). Similarly, later collisions took place concurrent with cooling of the bulk asteroid (as expected following the end of parent body metamorphism), and may or may not have played a role in first heating and then rapidly cooling down L-type material.

If all of the ages recorded by strong shocked meteorites are taken as representing impacts, three collisional events/periods are needed to explain our observations: early exhumation-driven cooling (4560–4530 Ma), collision(s) coincident with cooling of the parent body during waning parent body radiogenic metamorphism (4530–4500 Ma), and a relatively larger number of collisions that took place after this time (Fig. 8).

We consider two key possibilities for dynamical interpretation of the record: (A) An important dynamical excitation event took place between around 4450–4480 Ma, potentially Moon-formation or Giant Planet migration (Yin et al., 2014; Bottke et al., 2015; Mojzsis et al., 2019), producing a collision-age cluster in this time-frame. This is potentially supported by the clustering of strongly shocked L chondrite upper intercept ages at this time; (B) L chondrite phosphate U-Pb ages record a shoulder of monotonically declining collisional rates from around 4500 to 4400 Ma. Early collisional events were recorded less frequently as the parent asteroid was still mostly hotter than the temperature needed to induce Pb diffusion from the phosphate crystal lattice (Blackburn et al., 2017).

Uniquely linking the L chondrite U-Pb age record to particular dynamical interpretations is non-trivial. For example, the timings of each of the proposed dynamical perturbations that may have scattered rocky objects, caused collisions, and reset U-Pb ages remain debated. Recently proposed ages for the start of lunar crust differentiation – and hence a lower limit on the age of the Moon-forming impact – range from 4.51 Ga to 4.42 Ga (Barboni et al., 2017; Maurice et al., 2020). Similarly, models involving late Giant Planet migration call for instabilities within the first 100 Myr of Solar System history, but are for now broadly agnostic as to whether this event post- or pre-dated the Moon-forming impact (Clement et al., 2019; Mojzsis et al., 2019). As such, it is not yet possible to infer with confidence a link between any one of these dynamical propositions and the L chondrite U-Pb record.

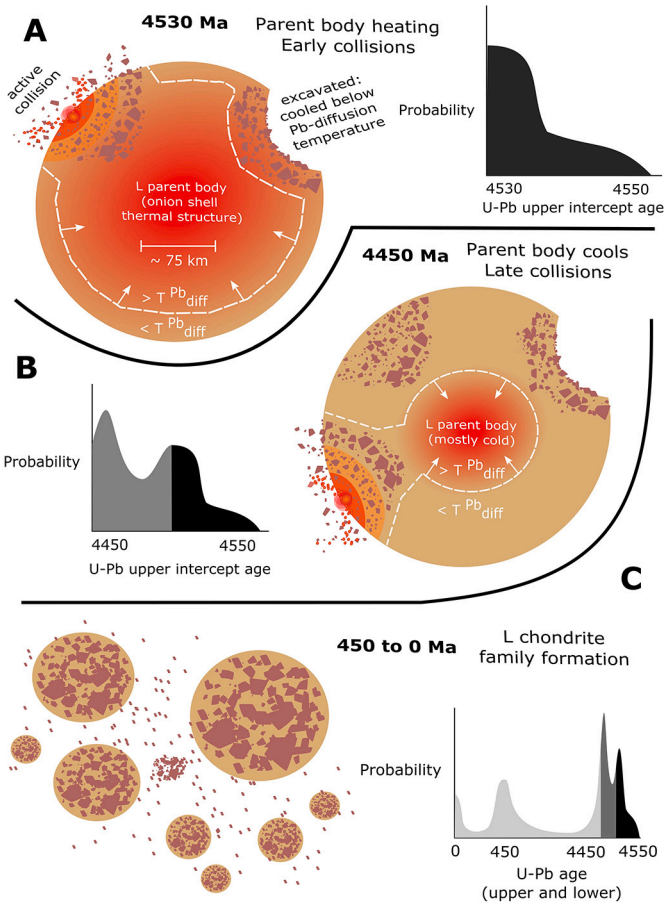

Fig. 8. Schematic evolution of the L chondrite parent asteroid. Schematic phosphate U-Pb age probability distributions that would be observed with complete sampling of the body, based on an interpretation of our results, are shown in each case. a) Initial evolution encompasses parent body formation, radiogenic heating, and the development of an onion-shell thermal structure (Blackburn et al., 2017; Edwards and Blackburn, 2020). b) Onion-shell age structure locked-in, but locally overprinted in case of impact events. c) After 4 billion years of relative collisional quiescence, the L asteroid was disrupted to create a family of smaller bodies at around 450 Ma.

An alternative to a solely dynamical interpretation is that the reorganisation of chondritic parent bodies into relatively porous rubble pile structures around 4460 Ma (Blackburn et al., 2017) changed the manner in which shock waves propagate through the parent body (Michel et al., 2003), dampening the extent to which shock metamorphism could have reset phosphate U-Pb ages. This possibility is difficult to evaluate at present, as rubble pile structure formation itself is also related to the dynamical state of the Solar System over time. Regardless, the complex links between these end-member interpretations highlight the need to link phosphate U-Pb age resetting behaviour with models that simultaneously and/or non-degenerately consider both broad dynamical and asteroid-specific variables.

Reconstructing the dynamical evolution of our Solar System by interpreting phosphate U-Pb upper intercept ages has great promise. The total available U-Pb upper intercept record for undifferentiated parent bodies lends tentative support to a shared collisional reheating feature at 4460–4480 Ma (Yin et al., 2014). However, sampling statistics for all parent bodies other than L chondrites remain poor. A wider sampling campaign is therefore needed to test whether this interpretation is statistically robust. What does seem clear, however, is that either collisional activity itself or the ability of L chondrite phosphate to record collisions dropped off after about 4440 Ma (Fig. 4). Upper intercept ages

from the L chondrites therefore provide evidence that collisional interactions in the inner Solar System changed in some way after 4440 Ma, potentially dating a terminal instability that greatly depleted the mass of the Main Belt (Clement et al., 2019; Ribeiro et al., 2020). This conclusion is independent of the nuances of interpretation of the earlier record, from 4460–4560 Ma, and provides evidence against the occurrence of a Late Heavy Bombardment between 4200–3800 Ma (Boehnke and Harrison, 2016).

4.3. Late stage break-up events

All but one of the lower intercept ages we present here (McKinney, within error of present day) are within error of a previously identified collisional age pulse inferred from Ar-Ar, K-Ar, and U-Pb analyses (Unruh, 1982; Korochantseva et al., 2007; Yin et al., 2014; Heck et al., 2017; Li and Hsu, 2018a,b,c; Schmitz et al., 2019) and the age (466 ± 1 Ma) of a sedimentary rock deposit that is strongly enriched in fossil L chondrite meteorites (Schmitz et al., 2019). A lunar impact event within error of our reconstructed age of the L parent body break-up event has also been dated by analysis of Apollo samples (Černok et al., 2021). Combined with our monitoring of possible sources of contamination (see Results), these observations suggest that L chondrite lower intercept ages are meaningful and record a collisional event at around this time.

We estimate the L parent body break-up event to have taken place at 474 ± 22 Ma (Fig. 3). Our best-estimate age is obtained by averaging all lower intercept ages with uncertainties of 50 Myr or less. Whilst the cut-off of 50 Myr uncertainty is arbitrary, this decision is informed by our previous finding that poorly constrained lower intercept ages for the Chelyabinsk meteorite were both inaccurate and imprecise (Popova et al., 2013; Lapen et al., 2014). It is on this basis that we exclude poorly constrained lower intercept ages from our best-estimate age for the L chondrite parent body break-up event (Fig. 3).

Statistical tests demonstrate the age distributions of lower intercept ages for weakly and strongly shocked meteorites to be indistinguishable (Fig. S8). This result is obtained even when the outlier sample McKinney is included (lower intercept age within error of present day), with the two populations becoming even more similar when McKinney is excluded. However, these same meteorites preserve upper intercept ages that differ by up to 100 Myr (and are not within error of one another; Fig. 4). This result is profound, suggesting that almost all L chondrite meteorites arriving at Earth over the last 500 Myr derive from a single rubble pile parent asteroid. This asteroid preserves a variety of U-Pb phosphate upper intercept ages throughout its structure and was broken up at 474 ± 22 Ma. Notably, there is no evidence from our results for the late heavy bombardment. In fact, the L chondrite collision age record is quiescent up from 4440 Ma until the break-up event recorded at 474 ± 22 Ma. This result is consistent to the growing body of evidence against any record of late heavy bombardment from analysis of many Solar System materials, including meteorites from the Moon and Vesta (Černok et al., 2021; Cartwright et al., 2022).

Why did a collisional event capable of disrupting an entire parent body not result in a distinguishable high-energy textural record in L chondrite meteorites? The presence of low shock features, e.g., irregular fractures, overprinting high-energy shock-related features, e.g., phosphate recrystallisation textures, in strongly shocked meteorites (Walton et al., 2022) (S5 and above) does evidence a textural record of more recent bombardment overprinting early events that took place at 4400–4600 Ma. The question, then, is whether features of such low shock stage can be consistent with an event of the scale needed to fragment a large asteroid parent body. However, simulations suggest that parent body fragmentation by impact of a comparatively small body is achievable without large scale melting or shock metamorphism of the target (Leinhardt and Stewart, 2009).

As noted earlier (section 4.2), if the L parent body that underwent disruption was already a porous rubble pile structure then it is also possible that the threshold energy of impact for disruption was relatively low, furthering the degree to which shock features at this time might not be produced in large volumes (Michel et al., 2003). Indeed, there are many examples of brecciated chondritic meteorites – requiring collisional reworking – that do not have high shock stages (Lentfort et al., 2021; Bischoff et al., 2018; Verdier-Paoletti et al., 2019). This general observation appears consistent with the concept of weak rubble pile structure chondritic asteroids undergoing fragmentation and brecciation with relative ease and frequency.

We conclude that the absence of evidence for shocking of material to high shock stages at 474 ± 22 Ma is potentially still consistent with evidence from U-Pb lower intercept ages for parent body disruption at this time. However, this scenario does place specific requirements on the physical properties of the L parent at the time and of the collision, which merits future scrutiny.

Lower intercept ages also provide evidence for potential continued collisional evolution of L chondrite families, with McKinney (L4, S5) recording an ejection event within error of the present day. This is analogous to the event recorded by the Chelyabinsk LL chondrite (Walton et al., 2022), evidence for recent fluid mobilisation within some carbonaceous chondrites (Turner et al., 2021), and may also be supported by evidence for modern Pb loss from ID-TIMS measurements of weakly shocked LL chondrites (Edwards and Blackburn, 2020). We rationalise the high frequency of L chondrites sampling the 474 ± 22 Ma collisional event relative to those samples recording geologically recent collisions as indicating something about the volumes of material reheated in the respective events recorded, i.e., a large volume of material reheated during parent body disruption and small volumes reheated during minor ejection events that have taken place with comparative frequency ever-since (Fig. 8c). Alternatively, McKinney may not record evidence for the 474 ± 22 Ma event due to originating from a different L type parent body.

Taken at face value, the L chondrite lower intercept record shows an apparent uptick in collision rate towards present day (i.e., samples recording lower intercept ages within error of zero age). However, this is currently based on very few samples. Contrary to the collisional event at 474 ± 22 Ma (Figs. 3–5), there is currently no complementary evidence from sedimentary deposits on Earth for either an increasing flux of extraterrestrial material, or specifically L material, over the last several 10s of Myr. Therefore, this apparent uptick may be a simple sampling artefact: material freshly shocked and ejected from its parent body soon arrives at Earth (Turner et al., 2021), where in general it has a very short window in which to be found or be destroyed by weathering. Evidence for short timescales of rubble pile resurfacing and/or ejecting collisions is mounting from observations of objects such as Bennu (Lauretta et al., 2019; Della Giustina et al., 2021). Furthermore, we have previously reported a lower intercept for Chelyabinsk (LL) within-error of present (Walton et al., 2022), indicating that recent and/or continuous minor collisional reworking may be prevalent for at least ordinary chondrite parent bodies.

4.4. Summary of L chondrite parent body evolution

Given available data, we can map out what appears to be the simplest interpretation of L chondrite parent body evolution. Fig. 8 illustrates schematic phosphate U-Pb age probability distributions that would be observed with complete sampling of the body (assuming only one initial progenitor, for now). Initial evolution encompasses parent body formation, radiogenic heating, and the development of an onion-shell thermal structure (Blackburn et al., 2017; Edwards and Blackburn, 2020) (Fig. 8a). By around 4530 Ma, the parent body begins to cool and phosphate U-Pb ages lock in the time at which rocks within the body cool down below the closure temperature for Pb-diffusion out of the apatite crystal lattice (Fig. 8a). Collisions in this timeframe may lock in ages early relative to the cooling rate expected from radiogenic decay

and heat diffusion for a given portion of the body, owing to excavation and subsequent rapid cooling of material.

From 4500–4450 Ma, the body has cooled in much of its outer portions. Now, only collisional reheating may drive Pb-diffusion from apatite located in most portions of the asteroid (Fig. 8b). At least one and perhaps several collisions took place at this time. These collisions may have reorganised the body into a partial or complete rubble pile. However, given the common origin and shared later collision history of most L chondrites, these events presumably did not create many bodies that actively feed Earth with L meteorites today. We envisage a body that partially retains its original onion shell structure and is partially mixed by impacts, enabling rapid cooling of some shocked components, e.g., McKinney (Fig. 8b). This period of collisional evolution ended around 4440 Ma, with our results revealing no (recorded) subsequent collisional events for the next 4 billion years.

After this long period of relative collisional quiescence, the L asteroid was disrupted to create a family of smaller bodies at around 474 ± 22 Ma (Fig. 8c). The vast majority of (but not all) L meteorites record this event, demonstrating their co-location within a single object at the time of disruption. Collisional evolution of the L family has continued until the present day, with L meteorites being common in collections and several rare samples recording ejecting collisions within error of the present day (Fig. 8c).

5. Conclusions

We measured in-situ phosphate U-Pb ages for nine L chondrite meteorites. Our results greatly increase the sampling density of the L parent asteroid U-Pb age distribution. We find that upper intercept U-Pb ages are correlated with shock stage, but lower intercept U-Pb ages are not. Upper intercept ages robustly record multiple early and severe collisional events. Lower intercepts record later mildly collisional events, including the break-up of an L parent body at 474 ± 22 Ma. In detail, our results reveal a complex history of collisional evolution for the L chondrite parent asteroid. We find that:

1. the L parent body experienced collisional reworking that resulted in the early cooling of some exhumed material (McKinney L6; 4567 Ma ± 20 Myr);
2. at least one later high-energy collision is recorded coincident with onion-shell cooling of weakly shocked, deeply buried, L6 samples at ≥ 4500 Ma (Blackburn et al., 2017). This result is consistent with reorganisation of the L asteroid into a rubble-pile structure by this time;
3. a second pulse of collisional evolution – at least one collisional event and possibly more than one – is identified at 4460–4480 Ma. This may be related to dynamical perturbation(s) of the inner Solar System at this time (Bottke et al., 2015; Mojzsis et al., 2019), but may also represent the shoulder of a monotonically declining collision rate inherent to the Main Belt;
4. L chondrites do not record any evidence of the late heavy bombardment, and suggest that collisional activity in the Solar System sharply declined at around 4440 Ma – potentially dating a terminal instability that greatly depleted the mass of the Main Belt (Clement et al., 2019; Ribeiro et al., 2020);
5. Lower intercept ages of L chondrites define a parent body break-up age of 474 ± 22 Ma.

Distinguishing between interpretations of our data and scenarios for the timing and origin of proposed dynamical changes will require fully quantitative models that link collision rates to asteroid phosphate U-Pb age distributions. These results could then be compared to the empirical record obtained by measuring meteorites.

A major event recorded by almost all of our samples (regardless of upper intercept age) and by previously studied L chondrites is recorded accurately but not precisely by lower intercept U-Pb ages at 474 ± 22 Ma. Combined with four previously measured lower intercept ages falling in the same window of time, our results are consistent with a parent body break-up event at this time (Schmitz et al., 2019). As such, L chondrite phosphate U-Pb ages provide evidence for a heterogeneous early and shared late (less than 500 Ma) thermal history for the majority of L-type meteorites falling to Earth today.

From this observation, we infer that most L chondrites derive from a single parent asteroid (in existence from at least 4500–4440 Ma to 474 ± 22 Ma), which has since been disturbed to create an asteroid family. This family continues to collisionally evolve to this day, evidence for which comes in the form of L chondrite meteorites with U-Pb lower intercept ages within error of the present day, similar to previously studied LL and carbonaceous chondrites (Turner et al., 2021; Walton et al., 2022). We conclude that L chondrite phosphate U-Pb ages map out a series of collisional events that span the entirety of Solar System history, from the birth of rocky objects to their continuing arrival at Earth today.

Declaration of competing interest

The authors declare that they have no known competing financial interests or personal relationships that could have appeared to influence the work reported in this paper.

Data availability

All of the data reported in this manuscript can be accessed in full at the NGDC by searching for entry FC48E70E06DE52E7E0530B37940A484D. This permanent data deposit includes BSE and SE images of phosphates before and after SIMS analysis, as well as CL images of many grains and a large number of whole section annotated BSE+EDS maps.

Acknowledgements

C.W. acknowledges NERC and UKRI for support through a NERC DTP studentship, grant number NE/L002507/1; financial support from the Cambridge Leverhulme center for Life in the Universe; funding support from Trinity College (Cambridge) in the form of a Junior Research Fellowship; funding support from ETH Zürich and the NOMIS formation in the form of a research fellowship. S.H. acknowledges support from the National Natural Science Foundation of China (grant number 41973062) and the key research program of the Institute of Geology and Geophysics, CAS (IGGCAS-201905). A.S.P.R. acknowledges support from Trinity College Cambridge. M.A. acknowledges funding from the UK Science and Technology Facilities Council (STFC) grants ST/P000657/1 and ST/T000228/. O.S. acknowledges support from the Isaac Newton Trust Early Career Support award. Dr Giulio Isacco Lampronti and Dr Iris Buisman are thanked with sincere gratitude for the many hours of technical support they provided during this project. Dr Martin Suttle is thanked for providing insightful comments on an early version of this manuscript. The NordSIMS facility is supported as a national infrastructure by the Swedish Research Council (grant 2017-00671). This manuscript is NordSIMS publication number 735. Dr Natasha Almeida, Dr Helena Bates, and all the staff involved in meteorite curation and sample preparation at the Natural History Museum (London) are thanked for their efforts, without which this work would not have been possible. NHM section numbers for the samples analysed in this study are noted in the supplementary materials associated with this manuscript, and in the permanently archived dataset stored with NGDC (https://www2.bgs.ac.uk/nationalgeosciencedatacentre/citedData/catalogue/a12602c6-51b0-459d-9b45-73dd93f6fa4d.html).

Appendix A. Supplementary material

Figures S1-6: Inverse concordia plots of apatite U-Pb isotopic data measured in this work. Figure S7: Further microtextural observations

of shocked phosphates in the Chelyabinsk meteorite (LL5). Figure S8: Further microtextural observations of shocked phosphates in the McKinney meteorite (L4). Figure S9: Further microtextural observations of shocked phosphates in the Isoulane-n-Amahar meteorite (L6). Figure S10: Further microtextural observations of shocked phosphates in the Chelyabinsk meteorite (LL5). Table S1: Research data including apatite U-Pb isotopic data measured in this study (see separate .csv file, 'Research 618 data Walton et al TableS1'). Supplementary material related to this article can be found online at https://doi.org/10.1016/j.gca.2023.07.012.

References

Barboni, M., Boehnke, P., Keller, B., Kohl, I.E., Schoene, B., Young, E.D., McKeegan, K.D., 2017. Early formation of the Moon 4.51 billion years ago. Sci. Adv. 3, e1602365. https://doi.org/10.1126/sciadv.1602365.

Baziotis, I., Asimow, P.D., Hu, J., Ferrière, L., Ma, C., Cernok, A., Anand, M., Topa, D., 2018. High pressure minerals in the Château-Renard (L6) ordinary chondrite: implications for collisions on its parent body. Sci. Rep. 8, 9851. https://doi.org/10.1038/s41598-018-28191-6.

Baziotis, I., Xydous, S., Papoutsa, A., Hu, J., Ma, C., Ferrière, L., Klemme, S., Berndt, J., Asimow, P., 2023. Investigation of the shocked Viñales ordinary chondrite (L6) meteorite fall – implications for shock classification, fragmentation, and collision dynamics. Icarus 390, 115326. https://doi.org/10.1016/j.icarus.2022.115326.

Bischoff, A., Schleiting, M., Wieler, R., Patzek, M., 2018. Brecciation among 2280 ordinary chondrites – constraints on the evolution of their parent bodies. Geochim. Cosmochim. Acta, 2189–2202. https://doi.org/10.1016/j.gca.2018.07.020.

Blackburn, T., Alexander, C.M., Carlson, R., Elkins-Tanton, L.T., 2017. The accretion and impact history of the ordinary chondrite parent bodies. Geochim. Cosmochim. Acta 200, 201–217. https://doi.org/10.1016/j.gca.2016.11.038.

Boehnke, P., Harrison, T.M., 2016. Illusory late heavy bombardments. Proc. Natl. Acad. Sci. 113, 10802–10806. https://doi.org/10.1073/pnas.1611535113.

Bottke, W.F., Vokrouhlický, D., Marchi, S., Swindle, T., Scott, E.R.D., Weirich, J.R., Levison, H., 2015. Dating the Moon-forming impact event with asteroidal meteorites. Science 348, 321–323. https://doi.org/10.1126/science.aaa0602.

Budde, G., Burkhardt, C., Kleine, T., 2019. Molybdenum isotopic evidence for the late accretion of outer Solar System material to Earth. Nat. Astron. 3, 736–741. https://doi.org/10.1038/s41550-019-0779-y.

Cartwright, J., Hodges, K., Wadhwa, M., 2022. Evidence against a Late Heavy Bombardment event on Vesta. Earth Planet. Sci. Lett. 590, 117576. https://doi.org/10.1016/j.epsl.2022.117576.

Černok, A., White, L.F., Anand, M., Tait, K.T., Darling, J.R., Whitehouse, M., Miljković, K., Lemelin, M., Reddy, S.M., Fougerouse, D., Rickard, W.D., Saxey, D.W., Ghent, R., 2021. Lunar samples record an impact 4.2 billion years ago that may have formed the Serenitatis Basin. Commun. Earth Environ. 2, 1–9. https://doi.org/10.1038/s43247-021-00181-z.

Černok, A., White, L.F., Darling, J., Dunlop, J., Anand, M., 2019. Shock-induced microtextures in lunar apatite and merrillite. Meteorit. Planet. Sci. 54, 1262–1282. https://doi.org/10.1111/maps.13278.

Clement, M.S., Morbidelli, A., Raymond, S.N., Kaib, N.A., 2019. A record of the final phase of giant planet migration fossilized in the asteroid belt's orbital structure. Mon. Not. R. Astron. Soc. 492, L56–L60. https://doi.org/10.1093/mnrasl/slz184.

Darling, J.R., Moser, D.E., Barker, I.R., Tait, K.T., Chamberlain, K.R., Schmitt, A.K., Hyde, B.C., 2016. Variable microstructural response of baddeleyite to shock metamorphism in young basaltic shergottite NWA 5298 and improved U–Pb dating of Solar System events. Earth Planet. Sci. Lett. 444, 1–12. https://doi.org/10.1016/j.epsl.2016.03.032.

Davison, T.M., O'Brien, D.P., Ciesla, F.J., Collins, G.S., 2013. The early impact histories of meteorite parent bodies. Meteorit. Planet. Sci. 48, 1894–1918. https://doi.org/10.1111/maps.12193.

Della Giustina, D.N., Kaplan, H.H., Simon, A.A., Bottke, W.F., Avdellidou, C., Delbo, M., Ballouz, R.L., Golish, D.R., Walsh, K.J., Popescu, M., Campins, H., Barucci, M.A., Poggiali, G., Daly, R.T., Corre, L.L., Hamilton, V.E., Porter, N., Jawin, E.R., McCoy, T.J., Connolly, H.C., Garcia, J.L.R., Tatsumi, E., Leon, J.d., Licandro, J., Fornasier, S., Daly, M.G., Asad, M.M.A., Philpott, L., Seabrook, J., Barnouin, O.S., Clark, B.E., Nolan, M.C., Howell, E.S., Binzel, R.P., Rizk, B., Reuter, D.C., Lauretta, D.S., 2021. Exogenic basalt on asteroid (101955) Bennu. Nat. Astron. 5, 31–38. https://doi.org/10.1038/s41550-020-1195-z.

Dodd, R., Jarosewich, E., 1979. Incipient melting in and shock classification of L-group chondrites. Earth Planet. Sci. Lett. 44, 335–340. https://doi.org/10.1016/0012-821x(79)90181-x.

Edwards, G.H., Blackburn, T., 2020. Accretion of a large LL parent planetesimal from a recently formed chondrule population. Sci. Adv. 6, eaay8641. https://doi.org/10.1126/sciadv.aay8641.

Erickson, T., Pearce, M., Taylor, R., Timms, N., Clark, C., Reddy, S., Buick, I., 2015. Deformed monazite yields high-temperature tectonic ages. Geology 43, 383–386. https://doi.org/10.1130/g36533.1.

Fritz, J., Greshake, A., Fernandes, V.A., 2017. Revising the shock classification of meteorites. Meteorit. Planet. Sci. 52, 1216–1232. https://doi.org/10.1111/maps.12845.

Gail, H.P., Trieloff, M., 2019. Thermal history modelling of the L chondrite parent body. Astron. Astrophys. 628, A77. https://doi.org/10.1051/0004-6361/201936020. arXiv:1907.00805.

Gattacceca, J., Suavet, C., Rochette, P., Weiss, B.P., Winklhofer, M., Uehara, M., Friedrich, J.M., 2014. Metal phases in ordinary chondrites: magnetic hysteresis properties and implications for thermal history. Meteorit. Planet. Sci. 49, 652–676. https://doi.org/10.1111/maps.12268.

Gyollai, I., Nagy, S., Fürj, J., Bérczi, S., Gucsik, A., Veres, M., 2009. Petrographic and micro-Raman study of thermal and shock metamorphism in Mezőmadaras, Knyahinya and Mócs L-chondrites. AIP Conf. Proc. 1163, 75–85. https://doi.org/10.1063/1.3222896.

Göpel, C., Manhès, G., Allègre, C.J., 1994. U-Pb systematics of phosphates from equilibrated ordinary chondrites. Earth Planet. Sci. Lett. 121, 153–171. https://doi.org/10.1016/0012-821x(94)90038-8.

Haba, M.K., Wotzlaw, J.F., Lai, Y.J., Yamaguchi, A., Schönbächler, M., 2019. Mesosiderite formation on asteroid 4 Vesta by a hit-and-run collision. Nat. Geosci. 12, 510–515. https://doi.org/10.1038/s41561-019-0377-8. arXiv:2103.16242.

Heck, P.R., Schmitz, B., Bottke, W.F., Rout, S.S., Kita, N.T., Cronholm, A., Defouilloy, C., Dronov, A., Terfelt, F., 2017. Rare meteorites common in the Ordovician period. Nat. Astron. 1, 0035. https://doi.org/10.1038/s41550-016-0035.

Hellmann, J.L., Kruijer, T.S., Orman, J.A.V., Metzler, K., Kleine, T., 2019. Hf-W chronology of ordinary chondrites. Geochim. Cosmochim. Acta 258, 290–309. https://doi.org/10.1016/j.gca.2019.05.040.

Hughes, J.M., Cameron, M., Crowley, K.D., 1989. Structural variations in natural F OH, and Cl apatites. Am. Mineral. 74, 870–876.

Jones, R.H., McCubbin, F.M., Dreeland, L., Guan, Y., Burger, P.V., Shearer, C.K., 2014. Phosphate minerals in LL chondrites: a record of the action of fluids during metamorphism on ordinary chondrite parent bodies. Geochim. Cosmochim. Acta 132, 120–140. https://doi.org/10.1016/j.gca.2014.01.027.

Jones, R.H., McCubbin, F.M., Guan, Y., 2016. Phosphate minerals in the H group of ordinary chondrites, and fluid activity recorded by apatite heterogeneity in the Zag H3-6 regolith breccia. Am. Mineral. 101, 2452–2467. https://doi.org/10.2138/am-2016-5728.

Kenny, G.G., Karlsson, A., Schmieder, M., Whitehouse, M.J., Nemchin, A.A., Bellucci, J.J., 2019. Recrystallization and chemical changes in apatite in response to hypervelocity impact. Geology 48, 19–23. https://doi.org/10.1130/g46575.1.

Korochantseva, E.V., Trieloff, M., Lorenz, C.A., Buykin, A.I., Ivanova, M.A., Schwarz, W.H., Hopp, J., Jessberger, E.K., 2007. Ar-Ar dating L chondrites. Meteorit. Planet. Sci. 42, 113–130. https://doi.org/10.1111/j.1945-5100.2007.tb00221.x.

Lapen, T.J., Kring, D.A., Zolensky, M., Andreasen, R., Righter, M., Swindle, T.D., Beard, S.P., 2014. Uranium-lead isotope evidence in the Chelyabinsk LL5 chondrite meteorite for ancient and recent thermal events. In: 45th Lunar and Planetary Science Conference.

Lauretta, D.S., DellaGiustina, D.N., Bennett, C.A., Golish, D.R., Becker, K.J., Balram-Knutson, S.S., Barnouin, O.S., Becker, T.L., Bottke, W.F., Boynton, W.V., Campins, H., Clark, B.E., Connolly, H.C., d'Aubigny, C.Y.D., Dworkin, J.P., Emery, J.P., Enos, H.L., Hamilton, V.E., Hergenrother, C.W., Howell, E.S., Izawa, M.R.M., Kaplan, H.H., Nolan, M.C., Rizk, B., Roper, H.L., Scheeres, D.J., Smith, P.H., Walsh, K.J., Wolner, C.W.V., Highsmith, D.E., Small, J., Vokrouhlický, D., Bowles, N.E., Brown, E., Hanna, K.L.D., Warren, T., Brunet, C., Chicoine, R.A., Desjardins, S., Gaudreau, D., Haltigin, T., Millington-Veloza, S., Rubi, A., Aponte, J., Gorius, N., Lunsford, A., Allen, B., Grindlay, J., Guevel, D., Hoak, D., Hong, J., Schrader, D.L., Bayron, J., Golubov, O., Sánchez, P., Stromberg, J., Hirabayashi, M., Hartzell, C.M., Oliver, S., Rascon, M., Harch, A., Joseph, J., Squyres, S., Richardson, D., Emery, J.P., McGraw, L., Ghent, R., Binzel, R.P., Asad, M.M.A., Johnson, C.L., Philpott, L., Susorney, H.C.M., Cloutis, E.A., Hanna, R.D., Connolly, H.C., Ciceri, F., Hildebrand, A.R., Ibrahim, E.M., Breitenfeld, L., Glotch, T., Rogers, A.D., Clark, B.E., Ferrone, S., Thomas, C.A., Campins, H., Fernandez, Y., Chang, W., Cheuvront, A., Trang, D., Tachibana, S., Yurimoto, H., Brucato, J.R., Poggiali, G., Pajola, M., Dotto, E., Epifani, E.M., Crombie, M.K., Lantz, C., Izawa, M.R.M., Leon, J.D., Licandro, J., Garcia, J.L.R., Clemett, S., Thomas-Keprta, K., Van wal, S., Yoshikawa, M., Bellerose, J., Bhaskaran, S., Boyles, C., Chesley, S.R., Elder, C.M., Farnocchia, D., Harbison, A., Kennedy, B., Knight, A., Martinez-Vlasoff, N., Mastrodemos, N., McElrath, T., Owen, W., Park, R., Rush, B., Swanson, L., Takahashi, Y., Velez, D., Yetter, K., Thayer, C., Adam, C., Antreasian, P., Bauman, J., Bryan, C., Carcich, B., Corvin, M., Geeraert, J., Hoffman, J., Leonard, J.M., Lessac-Chenen, E., Levine, A., McAdams, J., McCarthy, L., Nelson, D., Page, B., Pelgrift, J., Sahr, E., Stakkestad, K., Stanbridge, D., Wibben, D., Williams, B., Williams, K., Wolff, P., Hayne, P., Kubitschek, D., Barucci, M.A., Deshapriya, J.D.P., Fornasier, S., Fulchignoni, M., Hasselmann, P., Merlin, F., Praet, A., Bierhaus, E.B., Billett, O., Boggs, A., Buck, B., Carlson-Kelly, S., Cerna, J., Chaffin, K., Church, E., Coltrin, M., Daly, J., Deguzman, A., Dubisher, R., Eckart, D., Ellis, D., Falkenstern, P., Fisher, A., Fisher, M.E., Fleming, P., Fortney, K., Francis, S., Freund, S., Gonzales, S., Haas, P., Hasten, A., Hauf, D., Hilbert, A., Howell, D., Jaen, F., Jayakody, N., Jenkins, M., Johnson, K., Lefevre, M., Ma, H., Mario, C., Martin, K., May, C., McGee, M., Miller, B., Miller, C., Miller, G., Mirfakhrai, A., Muhle, E., Norman, C., Olds, R., Parish, C., Ryle, M., Schmitzer, M., Sherman, P., Skeen, M., Susak, M., Sutter, B., Tran, Q., Welch, C., Witherspoon, R., Wood, J., Zareski, J., Arvizu-Jakubicki, M., Asphaug, E., Audi, E., Ballouz, R.L., Bandrowski, R., Becker, K.J., Becker, T.L., Bendall, S., Bennett, C.A.,

Bloomenthal, H., Blum, D., Boynton, W.V., Brodbeck, J., Burke, K.N., Chojnacki, M., Colpo, A., Contreras, J., Cutts, J., d'Aubigny, C.Y.D., Dean, D., DellaGiustina, D.N., Diallo, B., Drinnon, D., Drozd, K., Enos, H.L., Enos, R., Fellows, C., Ferro, T., Fisher, M.R., Fitzgibbon, G., Fitzgibbon, M., Forelli, J., Forrester, T., Galinsky, I., Garcia, R., Gardner, A., Golish, D.R., Habib, N., Hamara, D., Hammond, D., Hanley, K., Harshman, K., Hergenrother, C.W., Herzog, K., Hill, D., Hoekenga, C., Hooven, S., Howell, E.S., Huettner, E., Janakus, A., Jones, J., Kareta, T.R., Kidd, J., Kingsbury, K., Balram-Knutson, S.S., Koelbel, L., Kreiner, J., Lambert, D., Lauretta, D.S., Lewin, C., Lovelace, B., Loveridge, M., Lujan, M., Maleszewski, C.K., Malhotra, R., Marchese, K., McDonough, E., Mogk, N., Morrison, V., Morton, E., Munoz, R., Nelson, J., Nolan, M.C., Padilla, J., Pennington, R., Polit, A., Ramos, N., Reddy, V., Riehl, M., Rizk, B., Roper, H.L., Salazar, S., Schwartz, S.R., Selznick, S., Shultz, N., Smith, P.H., Stewart, S., Sutton, S., Swindle, T., Tang, Y.H., Westermann, M., Wolner, C.W.V., Worden, D., Zega, T., Zeszut, Z., Bjurstrom, A., Bloomquist, L., Dickinson, C., Keates, E., Liang, J., Nifo, V., Taylor, A., Teti, F., Caplinger, M., Bowles, H., Carter, S., Dickenshied, S., Doerres, D., Fisher, T., Hagee, W., Hill, J., Miner, M., Noss, D., Piacentine, N., Smith, M., Toland, A., Wren, P., Bernacki, M., Munoz, D.P., Watanabe, S.i., Sandford, S.A., Aqueche, A., Ashman, B., Barker, M., Bartels, A., Berry, K., Bos, B., Burns, R., Calloway, A., Carpenter, R., Castro, N., Cosentino, R., Donaldson, J., Dworkin, J.P., Cook, J.E., Emr, C., Everett, D., Fennell, D., Fleshman, K., Folta, D., Gallagher, D., Garvin, J., Getzandanner, K., Glavin, D., Hull, S., Hyde, K., Ido, H., Ingegneri, A., Jones, N., Kaotira, P., Lim, L.F., Liounis, A., Lorentson, C., Lorenz, D., Lyzhoft, J., Mazarico, E.M., Mink, R., Moore, W., Moreau, M., Mullen, S., Nagy, J., Neumann, G., Nuth, J., Poland, D., Reuter, D.C., Rhoads, L., Rieger, S., Rowlands, D., Sallitt, D., Scroggins, A., Shaw, G., Simon, A.A., Swenson, J., Vasudeva, P., Wasser, M., Zellar, R., Grossman, J., Johnston, G., Morris, M., Wendel, J., Burton, A., Keller, L.P., McNamara, L., Messenger, S., Nakamura-Messenger, K., Nguyen, A., Righter, K., Queen, E., Bellamy, K., Dill, K., Gardner, S., Giuntini, M., Key, B., Kissell, J., Patterson, D., Vaughan, D., Wright, B., Gaskell, R.W., Corre, L.L., Li, J.Y., Molaro, J.L., Palmer, E.E., Siegler, M.A., Tricarico, P., Weirich, J.R., Zou, X.D., Ireland, T., Tait, K., Bland, P., Anwar, S., Bojorquez-Murphy, N., Christensen, P.R., Haberle, C.W., Mehall, G., Rios, K., Franchi, I., Rozitis, B., Beddingfield, C.B., Marshall, J., Brack, D.N., French, A.S., McMahon, J.W., Scheeres, D.J., Jawin, E.R., McCoy, T.J., Russell, S., Killgore, M., Bottke, W.F., Hamilton, V.E., Kaplan, H.H., Walsh, K.J., Bandfield, J.L., Clark, B.C., Chodas, M., Lambert, M., Masterson, R.A., Daly, M.G., Freemantle, J., Seabrook, J.A., Barnouin, O.S., Craft, K., Daly, R.T., Ernst, C., Espiritu, R.C., Holdridge, M., Jones, M., Nair, A.H., Nguyen, L., Peachey, J., Perry, M.E., Plescia, J., Roberts, J.H., Steele, R., Turner, R., Backer, J., Edmundson, K., Mapel, J., Milazzo, M., Sides, S., Manzoni, C., May, B., Delbo', M., Libourel, G., Michel, P., Ryan, A., Thuillet, F., Marty, B., 2019. The unexpected surface of asteroid (101955) Bennu. Nature 568, 55–60. https://doi.org/10.1038/s41586-019-1033-6.

Leinhardt, Z.M., Stewart, S.T., 2009. Full numerical simulations of catastrophic small body collisions. Icarus 199, 542–559. https://doi.org/10.1016/j.icarus.2008.09.013. arXiv:0811.0175.

Lentfort, S., Bischoff, A., Ebert, S., Patzek, M., 2021. Classification of CM chondrite breccias – implications for the evaluation of samples from the OSIRIS-REx and Hayabusa 2 missions. Meteorit. Planet. Sci. 56, 127–147. https://doi.org/10.1111/maps.13486.

Li, Q.L., Li, X.H., Wu, F.Y., Yin, Q.Z., Ye, H.M., Liu, Y., Tang, G.Q., Zhang, C.L., 2012. In-situ SIMS U–Pb dating of phanerozoic apatite with low U and high common Pb. Gondwana Res. 21, 745–756. https://doi.org/10.1016/j.gr.2011.07.008.

Li, S., Hsu, W., 2018a. Dating phosphates of the strongly shocked Suizhou chondrite. Am. Mineral. 103, 1789–1799. https://doi.org/10.2138/am-2018-6582.

Li, S., Hsu, W., 2018b. The nature of the L chondrite parent body's disruption as deduced from high-pressure phases in the Sixiangkou L6 chondrite. Meteorit. Planet. Sci. 53, 2107–2122. https://doi.org/10.1111/maps.13110.

Li, Y., Hsu, W., 2018c. Multiple impact events on the L-chondritic parent body: insights from SIMS U-Pb dating of Ca-phosphates in the NWA 7251 L-melt breccia. Meteorit. Planet. Sci. 53, 1081–1095. https://doi.org/10.1111/maps.13061.

Maurice, M., Tosi, N., Schwinger, S., Breuer, D., Kleine, T., 2020. A long-lived magma ocean on a young Moon. Sci. Adv. 6, eaba8949. https://doi.org/10.1126/sciadv.aba8949.

McGraw, A.M., Reddy, V., Sanchez, J.A., 2018. Do L chondrites come from the Gefion family? Mon. Not. R. Astron. Soc. 476, 630–634. https://doi.org/10.1093/mnras/sty250.

Mezger, K., Krogstad, E.J., 1997. Interpretation of discordant U-Pb zircon ages: an evaluation. J. Metamorph. Geol. 15, 127–140. https://doi.org/10.1111/j.1525-1314.1997.00008.x.

Michel, P., Benz, W., Richardson, D.C., 2003. Disruption of fragmented parent bodies as the origin of asteroid families. Nature 421, 608–611. https://doi.org/10.1038/nature01364.

Mojzsis, S.J., Brasser, R., Kelly, N.M., Abramov, O., Werner, S.C., 2019. Onset of giant planet migration before 4480 million years ago. Astrophys. J. 881, 44. https://doi.org/10.3847/1538-4357/ab2c03.

Nesvorný, D., Bottke Jr., W.F., Dones, L., Levison, H.F., 2002. The recent breakup of an asteroid in the main-belt region. Nature 417, 720–721. https://doi.org/10.1038/nature00789.

Ozawa, S., Ohtani, E., Suzuki, A., Miyahara, M., Terada, K., Kimura, M., 2007. Shock metamorphism of L6 chondrites Sahara 98222 and Yamato 74445: the PT conditions and the shock age. In: AGU Fall Meeting Abstracts.

Popova, O.P., Jenniskens, P., Emel'yanenko, V., Kartashova, A., Biryukov, E., Khaibrakhmanov, S., Shuvalov, V., Rybnov, Y., Dudorov, A., Grokhovsky, V.I., Badyukov, D.D., Yin, Q.Z., Gural, P.S., Albers, J., Granvik, M., Evers, L.G., Kuiper, J., Kharlamov, V., Solovyov, A., Rusakov, Y.S., Korotkiy, S., Serdyuk, I., Korochantsev, A.V., Larionov, M.Y., Glazachev, D., Mayer, A.E., Gisler, G., Gladkovsky, S.V., Wimpenny, J., Sanborn, M.E., Yamakawa, A., Verosub, K.L., Rowland, D.J., Roeske, S., Botto, N.W., Friedrich, J.M., Zolensky, M.E., Le, L., Ross, D., Ziegler, K., Nakamura, T., Ahn, I., Lee, J.I., Zhou, Q., Li, X.H., Li, Q.L., Liu, Y., Tang, G.Q., Hiroi, T., Sears, D., Weinstein, I.A., Vokhmintsev, A.S., Ishchenko, A.V., Schmitt-Kopplin, P., Hertkorn, N., Nagao, K., Haba, M.K., Komatsu, M., Mikouchi, T., the Chelyabinsk Airburst Consortium, 2013. Chelyabinsk airburst, damage assessment, meteorite recovery, and characterization. Science 342, 1069–1073. https://doi.org/10.1126/science.1242642.

Reddy, V., Sanchez, J.A., Bottke, W.F., Cloutis, E.A., Izawa, M.R., O'Brien, D.P., Mann, P., Cuddy, M., Corre, L.L., Gaffey, M.J., Fujihara, G., 2014. Chelyabinsk meteorite explains unusual spectral properties of Baptistina Asteroid Family. Icarus 237, 116–130. https://doi.org/10.1016/j.icarus.2014.04.027.

Ribeiro, R.d.S., Morbidelli, A., Raymond, S.N., Izidoro, A., Gomes, R., Neto, E.V., 2020. Dynamical evidence for an early giant planet instability. Icarus 339, 113605. https://doi.org/10.1016/j.icarus.2019.113605.

Righter, K., Abell, P., Agresti, D., Berger, E.L., Burton, A.S., Delaney, J.S., Fries, M.D., Gibson, E.K., Haba, M.K., Harrington, R., Herzog, G.F., Keller, L.P., Locke, D., Lindsay, F.N., McCoy, T.J., Morris, R.V., Nagao, K., Nakamura-Messenger, K., Niles, P.B., Nyquist, L.E., Park, J., Peng, Z.X., Shih, C., Simon, J.I., Swisher, C.C., Tappa, M.J., Turrin, B.D., Zeigler, R.A., 2015. Mineralogy, petrology, chronology, and exposure history of the Chelyabinsk meteorite and parent body. Meteorit. Planet. Sci. 50, 1790–1819. https://doi.org/10.1111/maps.12511.

Schlichting, H.E., Warren, P.H., Yin, Q.Z., 2012. The last stages of terrestrial planet formation: dynamical friction and the late veneer. Astrophys. J. 752, 8. https://doi.org/10.1088/0004-637x/752/1/8.

Schmitz, B., Farley, K.A., Goderis, S., Heck, P.R., Bergström, S.M., Boschi, S., Claeys, P., Debaille, V., Dronov, A., Ginneken, M.v., Harper, D.A., Iqbal, F., Friberg, J., Liao, S., Martin, E., Meier, M.M.M., Peucker-Ehrenbrink, B., Soens, B., Wieler, R., Terfelt, F., 2019. An extraterrestrial trigger for the mid-Ordovician ice age: dust from the breakup of the L-chondrite parent body. Sci. Adv. 5, eaax4184. https://doi.org/10.1126/sciadv.aax4184.

Stacey, J., Kramers, J., 1975. Approximation of terrestrial lead isotope evolution by a two-stage model. Earth Planet. Sci. Lett. 26, 207–221. https://doi.org/10.1016/0012-821x(75)90088-6.

Stöffler, D., Hamann, C., Metzler, K., 2018. Shock metamorphism of planetary silicate rocks and sediments: proposal for an updated classification system. Meteorit. Planet. Sci. 53, 5–49. https://doi.org/10.1111/maps.12912.

Stöffler, D., Keil, K., Scott, E.R.D., 1991. Shock metamorphism of ordinary chondrites. Geochim. Cosmochim. Acta 55, 3845–3867. https://doi.org/10.1016/0016-7037(91)90078-j.

Taylor, G.J., Maggiore, P., Scott, E.R., Rubin, A.E., Keil, K., 1987. Original structures, and fragmentation and reassembly histories of asteroids: evidence from meteorites. Icarus 69, 1–13. https://doi.org/10.1016/0019-1035(87)90002-9.

Terada, K., Bischoff, A., 2009. Asteroidal granite-like magmatism 4.53 Gyr ago. Astrophys. J. 699, L68–L71. https://doi.org/10.1088/0004-637x/699/2/l68.

Trieloff, M., Jessberger, E.K., Herrwerth, I., Hopp, J., Fiéni, C., Ghélis, M., Bourot-Denise, M., Pellas, P., 2003. Structure and thermal history of the H-chondrite parent asteroid revealed by thermochronometry. Nature 422, 502–506. https://doi.org/10.1038/nature01499.

Turner, S., McGee, L., Humayun, M., Creech, J., Zanda, B., 2021. Carbonaceous chondrite meteorites experienced fluid flow within the past million years. Science 371, 164–167. https://doi.org/10.1126/science.abc8116.

Unruh, D., 1982. The UThPb age of equilibrated L chondrites and a solution to the excess radiogenic Pb problem in chondrites. Earth Planet. Sci. Lett. 58, 75–94. https://doi.org/10.1016/0012-821x(82)90104-2.

Verdier-Paoletti, M.J., Marrocchi, Y., Vacher, L.G., Gattacceca, J., Gurenko, A., Sonzogni, C., Gounelle, M., 2019. Testing the genetic relationship between fluid alteration and brecciation in CM chondrites. Meteorit. Planet. Sci. 54, 1692–1709. https://doi.org/10.1111/maps.13306.

Vermeesch, P., 2018. IsoplotR: a free and open toolbox for geochronology. Geosci. Front. 9, 1479–1493. https://doi.org/10.1016/j.gsf.2018.04.001.

Vokrouhlický, D., Bottke, W.F., Nesvorný, D., 2017. Forming the Flora family: implications for the near-Earth asteroid population and large terrestrial planet impactors. Astron. J. 153, 172. https://doi.org/10.3847/1538-3881/aa64dc.

Walton, C.R., Baziotis, I., Černok, A., Ludovic, F., Asimow, P.D., Shorttle, O., Anand, M., 2021. Microtextures in the Chelyabinsk impact breccia reveal the history of Phosphorus-Olivine-Assemblages in chondrites. Meteorit. Planet. Sci. 56, 742–766. https://doi.org/10.1111/maps.13648.

Walton, C.R., Shorttle, O., Hu, S., Rae, A.S.P., Jianglong, J., Černok, A., Williams, H., Liu, Y., Tang, G., Li, Q., Anand, M., 2022. Ancient and recent collisions revealed by phosphate minerals in the Chelyabinsk meteorite. Commun. Earth Environ. 3, 40. https://doi.org/10.1038/s43247-022-00373-1.

Wu, Y., Hsu, W., 2019. Petrogenesis and in situ U-Pb geochronology of a strongly shocked L-Melt rock Northwest Africa 11042. J. Geophys. Res., Planets 124, 893–909. https://doi.org/10.1029/2018JE005743.

Xie, X., Chen, M., Wang, D., 2001. Shock-related mineralogical features and P-T history of the Suizhou L6 chondrite. Eur. J. Mineral. 13, 1177–1190. https://doi.org/10.1127/0935-1221/2001/0013-1177.

Xie, X., Yang, H., Gu, X., Downs, R.T., 2015. Chemical composition and crystal structure of merrillite from the Suizhou meteorite. Am. Mineral. 100, 2753–2756. https://doi.org/10.2138/am-2015-5488.

Yin, Q., Zhou, Q., Li, Q., Li, X., Liu, Y., Tang, G., Krot, A.N., Jenniskens, P., 2014. Records of the Moon-forming impact and the 470 Ma disruption of the L chondrite parent body in the asteroid belt from U-Pb apatite ages of Novato (L6). Meteorit. Planet. Sci. 49, 1426–1439. https://doi.org/10.1111/maps.12340.

Zhou, Q., Herd, C.D., Yin, Q.Z., Li, X.H., Wu, F.Y., Li, Q.L., Liu, Y., Tang, G.Q., McCoy, T.J., 2013. Geochronology of the Martian meteorite Zagami revealed by U–Pb ion probe dating of accessory minerals. Earth Planet. Sci. Lett. 374, 156–163. https://doi.org/10.1016/j.epsl.2013.05.035.